

Dear editor,

Thank you very much for your valuable review and point-by-point comments. We have revised the manuscript carefully following your comments and suggestions. The revised manuscript and the supplemental material with marked changes are included as follow.

Sincerely,

Lei Cai, on behalf of all coauthors.

1 **Projecting circum-Arctic excess ground ice melt with a sub-grid representation in the Community**  
2 **Land Model**

3 Lei Cai<sup>1</sup>, Hanna Lee<sup>1</sup>, Kjetil Schanke Aas<sup>2</sup>, Sebastian Westermann<sup>2</sup>

4 <sup>1</sup>NORCE Norwegian Research Centre, Bjerknes Centre for Climate Research, 5008, Bergen, Norway

5 <sup>2</sup>Department of Geosciences, University of Oslo, Oslo, 0315, Norway

6 *Correspondence to:* Lei Cai (leca@norceresearch.no)

7 **Abstract** To address the longstanding underrepresentation of the influences of highly variable ground  
8 ice content on the trajectory of permafrost conditions simulated in Earth System Models under a warming  
9 climate, we implement a sub-grid representation of excess ground ice within permafrost soils using the  
10 latest version of the Community Land Model (CLM5). Based on the original CLM5 tiling hierarchy, we  
11 duplicate the natural vegetated landunit by building extra tiles for up to three cryostratigraphies with  
12 different amounts of excess ice for each grid cell. For the same total amount of excess ice, introducing  
13 sub-grid variability in excess ice contents leads to different excess ice melting rates at the grid level. In  
14 addition, there are impacts on permafrost thermal properties and local hydrology with sub-grid  
15 representation. We evaluate this new development with single-point simulations at the Lena river delta,  
16 Siberia, where three sub-regions with distinctively different excess ice conditions are observed. A triple-  
17 landunit case accounting for this spatial variability conforms well to previous model studies for the Lena  
18 river delta and displays a markedly different dynamics of future excess ice thaw compared to a single-  
19 landunit case initialized with average excess ice contents. For global simulations, we prescribed a tiling  
20 scheme combined with our sub-grid representation to the global permafrost region [using presently](#)  
21 [available circum-Arctic ground ice data](#)~~using the dataset “Circum-Arctic Map of Permafrost and Ground-~~  
22 ~~Ice Conditions” (Brown et al., 1997)~~. The sub-grid scale excess ice produces significant melting of excess  
23 ice under a warming climate and enhances the representation of sub-grid variability of surface subsidence  
24 on a global scale. Our model development makes it possible to portray more details on the permafrost  
25 degradation trajectory depending on the sub-grid soil thermal regime and excess ice melting, which also  
26 shows a strong indication that accounting for excess ice is a prerequisite of a reasonable projection of  
27 permafrost thaw. The modeled permafrost degradation with sub-grid excess ice follows the pathway that  
28 continuous permafrost transforms into discontinuous permafrost before it disappears, including surface  
29 subsidence and talik formation, which are highly permafrost-relevant landscape changes excluded from  
30 most land models. Our development of sub-grid representation of excess ice demonstrates a way forward  
31 to improve the realism of excess ice melt in global land models, but further developments [require](#)  
32 [substantially improved](#)~~rely on additional~~ global observational datasets on both the horizontal and vertical  
33 distributions of excess ground ice.

## 34 1. Introduction

35 Permafrost soils are often characterized by different types of ground ice that can exceed the pore  
36 space (Brown et al. 1997; Zhang et al., 1999). The presence of such “excess” ground ice can alter the  
37 permafrost thermal regime and landscape structure. Widespread thawing of permafrost is expected in a  
38 warmer future climate and modeling studies suggest large-scale degradation of near-surface permafrost  
39 at the end of the 21st century (Lawrence et al., 2008 & 2011). Melting of ground ice due to active layer  
40 thickening releases water [in the form of surface runoff, subsurface flow, or both, causing in the form of](#)  
41 [surface and/or subsurface runoff, causing](#) surface subsidence and modifying the local hydrological cycle  
42 (West and Plug, 2008; Grosse et al., 2011; Kokelj et al., 2013; Westermann et al., 2016). In addition to  
43 containing ground ice, some permafrost soils store massive amounts of carbon, which could be released  
44 to the atmosphere in the form of greenhouse gases upon thawing (Walter et al., 2006; Zimov et al., 2006;  
45 Schuur et al., 2008), possibly making a positive feedback to amplify future climate change (Koven et al.,

46 2011; Schaefer et al., 2014; Burke et al., 2013). The existence of excess ice and its distribution in  
47 permafrost can significantly affect the rate of permafrost thawing (Westermann et al., 2016; Nitzbon et  
48 al., 2020), and in turn, the rate of soil carbon release (Hugelius et al., 2014; Schuur et al., 2015; Turetsky  
49 et al., 2019). Therefore, better projections of excess ice melt are critical to improve our understanding of  
50 the impacts of permafrost thaw on corresponding climatic impacts.

51 Previous studies address excess ice modeling on the local or regional scale, in which the small study  
52 area makes it possible for detailed configurations of the cryostratigraphy of permafrost and excess ice  
53 based on observations. Simulations for the Lena river delta have retrieved the permafrost thermal  
54 dynamics fairly close to the observations with excess ice incorporated in the modeling (Westermann et  
55 al., 2016). A two-tile approach allowing lateral heat exchange between two land elements demonstrated  
56 that maintaining thermokarst ponds requires the heat loss from water to the surrounding land (Langer et  
57 al., 2016). A similar tiling approach has been applied to projecting the landscape changes due to  
58 permafrost thaw for ice-wedge polygons and peat plateaus with different features of ice melting and  
59 surface subsidence (Aas et al., 2019; Nitzbon et al., 2019).

60 On the global scale, the land components of Earth System Models (ESMs) have significant  
61 capabilities of representing key permafrost physics. In the Community Land Model (CLM), for example,  
62 the representation of permafrost-associated processes has been continuously ~~improving~~ <sup>improving</sup>. By including  
63 key thermal and hydrological processes of permafrost, the CLM version 4 (CLM4) has reasonably  
64 reproduced the global distribution of permafrost (Lawrence et al., 2008; Lawrence et al., 2012; Slater  
65 and Lawrence, 2013). Projections based on the CLM4 under its highest warming scenario (RCP8.5) have  
66 shown over 50% degradation of near-surface permafrost by 2100 (Lawrence et al., 2012). Moreover, the  
67 recently released CLM5 has more advanced representations of many biogeophysical and biogeochemical  
68 processes (Lawrence et al., 2019). A refined soil profile and upgraded snow accumulation and  
69 densification scheme in the CLM5 could contribute to simulating more realistic permafrost thermal  
70 regimes, whereas upgrades on biogeochemistry improve simulations of soil carbon release in response  
71 to permafrost thaw. In addition, an excess ice physics scheme has been implemented in CLM4.5  
72 (CLM4.5\_EXICE) by Lee et al. (2014), which allowed for the first-order simulation of surface  
73 subsidence globally by modeling excess ice melt under a warming climate.

74 The homogeneous distribution of excess ice throughout the grid cell in CLM4.5\_EXICE (Lee et al.,  
75 2014) could cause biases in thaw trajectories in the warming climate. In nature, excess ice forms in a  
76 highly localized manner due to a variety of accumulation processes. For instance, segregated ice formed  
77 during frost heave differs substantially in excess ice morphology from ice wedges that are formed from  
78 repeated frost cracking and freezing of penetrating water. Field measurements illustrate that the depth  
79 distribution of ground ice can vary substantially on the order to 10-50 ~~meters-mctres~~ horizontally and 0-  
80 10 ~~metrcers~~ vertically (Pascale et al., 2008; Fritz et al., 2011). The horizontal grid spacing of ESMs, on  
81 the other hand, usually ranges from one to two degrees (~100-200 km horizontal scale), which makes it  
82 impossible to represent localized excess ice. The mismatch in spatial scale between model and the real  
83 world raises concerns for the reliability of excess ice modeling in ESMs. Aside from the homogeneously

84 -initialized excess ice in the grid cell, CLM4.5\_EXICE initializes excess ice in the same soil depths  
85 globally (below 1m), regardless of the varying active layer thickness in circum-Arctic permafrost areas  
86 (Lee et al., 2014). Such deficiencies in excess ice parameterization hamper global projections of  
87 permafrost thaw including excess ice with ESMs.

88 To narrow the gap between the high spatial variability of excess ice and the coarse grid spacing in  
89 the ESMs, we applied a sub-grid approach in representing excess ice in permafrost soils within the CLM5  
90 to investigate how presence and melting of excess ice affect land surface physics under a warming climate.  
91 We conducted idealized single-point simulations to examine the robustness of model development. ~~We~~  
92 ~~and~~ furthermore conducted global simulations using a first-order estimate for the spatial distribution of  
93 excess ice and associated cryostratigraphies. ~~, aiming to present a model framework that can eventually~~  
94 ~~bring the modeling towards a higher accuracy.~~ Due to the lack of information in global excess ice  
95 conditions, it is not the aim of this study to accurately project excess ice melt and surface subsidence in  
96 the 21st century, but rather to develop ~~and present~~ a functional process within a land surface model  
97 ~~that can eventually bring permafrost thaw modeling towards a higher degree of accuracy~~ on a global  
98 scale. The CLM5 with sub-grid excess ice representation developed through this study would be ready  
99 to serve as a proper simulation tool on further advancing global excess ice modeling once new datasets  
100 become available.

## 101 2. Methodology

### 102 2.1 Sub-grid representation of excess ice in the CLM5

103 The CLM5 model utilizes a three-level tiling hierarchy to represent sub-grid heterogeneity of  
104 landscapes, which are (from top to bottom) landunits, columns, and patches (Lawrence et al., 2019).  
105 There is only one column (the natural soil column) that is under the natural vegetated landunit, which  
106 represents soil including permafrost. In this study, we modify the CLM5 tiling hierarchy by duplicating  
107 the natural vegetated landunit, making extra landunits for prescribing up to three different excess ice  
108 conditions in permafrost (Figure 1). The original natural vegetated landunit is considered as “natural  
109 vegetated with no excess ice” (hereafter no ice landunit), while we denote the additional landunits as  
110 “natural vegetated with low content of excess ice” (hereafter the low ice landunit), “natural vegetated  
111 with medium content of excess ice” (hereafter the mid ice landunit), and “natural vegetated with high  
112 content of excess ice” (hereafter the high ice landunit). The sub-grid initial conditions of excess ice are  
113 imported as part of the surface data, which includes the variables of volumetric excess ice contents,  
114 depths of the top and bottom soil layer of added excess ice, and the area weights of the four landunits.

115 We adopted the excess ice physics from CLM4.5\_EXICE (Lee et al., 2014), including  
116 thermodynamic and hydrological processes. The added excess ice is evenly distributed within each soil  
117 layer. ~~Note that~~ ~~Whereas~~ the original CLM5 model already represents the dynamics of pore ice. ~~Our, our~~  
118 representation of excess ice physics only addresses the ground ice bodies that exceed soil pore space.  
119 The volumetric excess ice content in this study is defined as the ratio of the volume of excess ice in a soil

120 layer to the volume of the whole soil layer. For example, a 50% volumetric content of excess ice means  
121 the excess ice body occupies 50% volume of a soil layer, while the rest of soil (and pore ice) occupies  
122 the other 50% volume of the soil layer. If not otherwise notified, the parameter of volumetric ice content  
123 in this manuscript refers only to that of excess ice bodies. After adding excess ice, the soil layer thickness  
124 increases accordingly. Because ice density is considered constant, the increase of soil layer thickness is  
125 linearly proportional to the volumetric content of excess ice. For example, adding an excess ice body  
126 with a 50% volumetric excess ice content doubles the soil layer thickness of the corresponding soil layer.  
127 The revised algorithm for thermal conductivity and heat capacity of soil involves the effects of added  
128 excess ice, while the revised phase change energy equation allows excess ice to melt. The meltwater adds  
129 to soil liquid water in the same soil layer, and it can move to the above layer if the original layer is  
130 saturated. Such numerical implementation replicates how the melt excess ice eventually converts to  
131 runoff and discharges from the soil in case of well-drained conditions. As excess ice melts, soil layer  
132 thickness decreases, which corresponds to surface subsidence due to excess ice melt. In our model  
133 parameterization, excess ice only melts and does not re-form since the applied excess ice physics does  
134 not account for the different ice formation processes.

135 Aside from sub-grid tiles for excess ice, we acknowledge that the version upgrade from CLM4.5 to  
136 CLM5 as the base model modifies the results of excess ice melt compared to the results from Lee et al.  
137 (2014). By default, CLM5 represents soil with a 25-layer profile, for which the top 20 hydrologically-  
138 active layers cover 8.5 metres of soil. There are additional 10 soil layers and it is 4.7 metres deeper  
139 compared to the default hydrologically-active soil layer profile in CLM4.5, not to mention the  
140 substantially more complex biogeophysical processes (Lawrence et al., 2019). Therefore, we developed  
141 the sub-grid representation of excess ice within the framework of the latest version of CLM. The  
142 duplicated landunits prolong computation time by roughly 10% compared to the original CLM5. We are,  
143 therefore, confident that our model development is highly efficient in addressing the sub-grid excess ice  
144 and subsequent permafrost thaw.

145 We examined the sensitivity of sub-grid excess ice initialization by conducting idealized  
146 experiments (see supplemental material). For overall the same amount of excess ice in one grid cell  
147 located in the same depth, a higher volumetric excess ice content along with a smaller area weight results  
148 in a later start of excess ice melt and a smaller melting rate. The different melting features from different  
149 sub-grid distribution of excess ice then leads to different hydrological impacts to the permafrost soil. The  
150 idealized experiments in this way verify the necessity of involving sub-grid configuration of excess ice  
151 to the CLM that is with a typical horizontal grid spacing of 1-2 degrees. More details are available in the  
152 supplemental material.

**Commented [LC1]:** We have added some stuff about the sensitivity test in the supplemental material.

## 153 2.2 Single-point simulations for the Lena river delta, Siberia

154 We conduct single-point simulations for the Lena River delta and compare the CLM5 model results  
155 to reference simulations with the CryoGrid3 model for the same location (Westermann et al., 2016).  
156 Abundant background information is available on the soil and ground ice dynamics from both  
157 observation and modeling, making the Lena river delta a suitable location to further evaluate our model

158 development. The Lena river delta can be broadly categorized into three different geomorphological units  
159 that have distinctively different subsurface cryostratigraphies of excess ice (Schneider et al., 2009; Ulrich  
160 et al., 2009). In the eastern and central part of the river delta, ground ice has been accumulated in the  
161 comparatively warm Holocene climate. The subsurface sediments (hereafter denoted as “Holocene  
162 ground ice terrain”) are generally super-saturated with wedge ice that can extend up to 9 metres  
163 underground with the volumetric contents of total ground ice (pore ice + excess ice) ranging from 60-  
164 80% (Schwamborn et al., 2002; Langer et al., 2013). On the other hand, higher excess ice contents are  
165 found in Pleistocene sediments in the Lena River Delta (hereafter the “Yedoma Ice complex”), which  
166 are characterized by Yedoma type ground ice (Schirrmeister et al., 2013), which can reach depths of up  
167 to 20-25 metres deep and volumetric contents of total ground ice as high as 90% (Schwamborn et al.,  
168 2002; Schirrmeister et al., 2003 and 2011). Finally, the Northwestern part of the delta features sandy  
169 sediments and is characterized by low excess ice contents (hereafter denoted the “no excess ice terrain”;  
170 Rachold and Grigoriev, 1999; Schwamborn et al., 2002).

171 We determine the area weights of excess ice landunits in one single point based on the spatial pattern  
172 of three subregions (Fedorova et al., 2015). The cryostratigraphy and the volumetric contents of excess  
173 ice strictly follow those in Westermann et al. (2016). Note that the excess ice initialization scenario  
174 in Westermann et al. (2016) does not necessarily represent the realistic excess ice condition for the Lena  
175 river delta. The purpose of applying the same excess ice cryostratigraphy as in Westermann et al. (2016)  
176 is to evaluate our model development by addressing intercomparisons between model results. Meanwhile,  
177 we did not customize soil properties for different landunits as in Westermann et al. (2016), as our model  
178 development does not support varying soil properties for different sub-grid landunits. We also directly  
179 apply the snow accumulation physics in the CLM rather than customizing the snow density. By default,  
180 the current model does not form thermokarst lakes as the meltwater from excess ice melt becomes surface  
181 runoff and is removed from the grid cell. To apply the sub-grid representation, we initialize the case with  
182 three landunits (the triple-landunit case) that respectively represent the three terraces in the Lena river  
183 delta. We also initialize an “average ice single-landunit” case without the sub-grid representation of  
184 excess ice. The excess ice amount for each soil layer in the average ice single-landunit case is initially  
185 the same as that in the triple-landunit case. The volumetric content of excess ice is determined by spatial  
186 averaging those for three excess ice landunits in the triple-landunit case. Detailed information on the  
187 applied excess ice conditions for both cases is listed in Table 1.

188 We employed the single-point forcing data from in Westermann et al. (2016) for the Lena river delta  
189 from 1901 to 2100, which is based on the CRU-NCEP (<http://dods.extra.cea.fr/data/p529viov/cruncep/>)  
190 data set for the historical period (1901-2005) and the CCSM4 model output under the RCP4.5 scenario  
191 for the projected period (2006-2100), but downscaled with in-situ observations. We run 100-year spin-  
192 up simulations in order to stabilize the permafrost thermal regime after adding excess ice. Spin-up  
193 simulations are produced by running the model with cycled 1901-1920 climatological data. The purpose  
194 of spin-up simulations is to stabilize ground temperatures and volumes of excess ice bodies. The 100-  
195 year length for spin-up is sufficient, as the model is run in Satellite Phenology (SP) mode that does not  
196 involve slowly evolving biogeochemical processes such as soil carbon accumulation. Moreover, we

197 address idealized single-point simulations for additional permafrost locations with both continental and  
198 maritime climate that showcase the difference to Lee et al. (2014), the results of which are included in  
199 the Supplementary material.

### 200 2.3 Global simulations of excess ice melt

201 The information available for the spatial distribution of excess ice and associated cryostratigraphies  
202 on the global scale is generally not as detailed as in the Lena river delta due to the lack of observations.  
203 For our global simulations we employ the widely used “Circum-Arctic Map of Permafrost and Ground-  
204 Ice Conditions” (hereafter the CAPS data; Brown et al., 2002) as data source, while we translate the  
205 ground ice condition in the CAPS data to different excess ice stratigraphies as model input data. The  
206 CAPS permafrost map categorizes the global permafrost area into classes coded by three factors (i)  
207 permafrost extent (c = continuous, d = discontinuous, s = sporadic, and i = isolated), (ii) visible ground  
208 ice content (h = high, m = medium, and l = low), and (iii) terrain and overburden (f = lowlands, highlands,  
209 and intra- and intermontane depressions characterized by thick overburden cover, and r = mountains,  
210 highlands ridges, and plateaus characterized by thin overburden cover and exposed bedrock), resulting  
211 in more than 20 different varieties in permafrost characteristics (Figure 2). For the simulations, we only  
212 use the CAPS distinction between the three classes: high, medium and low ice contents. We qualitatively  
213 categorize excess ice types with typical cryostratigraphies for which observations are available,  
214 recognizing that this is a crude first-guess of the global distribution of ground ice which needs to be  
215 improved in future studies.

216 The high ice CAPS classes (e.g. chf, chr, and dhf) in central and eastern Siberia, as well as in Alaska,  
217 partly coincide with Yedoma regions (Kanevskiy et al., 2011; Grosse et al., 2013). The cryostratigraphy  
218 of the high ice landunit is therefore broadly oriented at the excess ice contents and distribution in intact  
219 Yedoma, which is characterized by massive ice wedges leading to typical average volumetric content of  
220 total ground ice in the range from 60% to 90% (Schwamborn et al., 2002; Kanevskiy et al., 2011). We  
221 therefore set the volumetric content of excess ice in the high ice landunit to 70%, and we put excess ice  
222 in all the soil layers between 0.2 metreers below the active layer and the bottom of hydrologically-  
223 soil layer (8.5 metreers). The onset depth of the excess ice just below the active layer is based on the  
224 assumption of active ice aggradation which occurs at or below the permafrost table, e.g. the formation of  
225 wedge or segregation ice. Initializing high ~~econtent~~-excess ice content throughout the whole soil layer  
226 imitates the cryostratigraphy of Yedoma type ice, while ~~a-certain amoun~~roughly 65% of the high ice  
227 landunit ~~loeaates-is located~~ out of the observed Yedoma regions (Schuur et al., 2015). The effects,  
228 limitations, and potential improvements of this initialization scenario will be mentioned in the discussion  
229 section. For the low ice landunit, we assume both a significantly lower volumetric excess ice content and  
230 a smaller vertical extent of the excess ice body. The volumetric excess ice content is set to 25%, and we  
231 add excess ice at soil layers within 0.2 to 1.2 metreers below the active layer, which in particular  
232 represents sediments with segregated ice (e.g. Cable et al., 2018), but also accounts for a wide range of  
233 different excess ice conditions found throughout the permafrost domain. For the mid ice landunit, we  
234 set the volumetric excess ice content to 45% and put excess ice within 0.2 to 2.2 metreers below the

235 active layer, making the volumetric excess ice content and vertical extent of which in between those for  
236 the low and high ice landunits. The cryostratigraphies determine that excess ice melt in the low ice  
237 landunit can result in a maximum of 0.36 metres of surface subsidence, while excess ice melt in the  
238 medium ice landunit can result in a maximum of 1.78 m of surface subsidence. For the high ice landunit,  
239 the surface subsidence can be more than 10 metres if all excess ice melts, which is expected to vary in  
240 space because of the different active layer thickness. For all three landunits, the active layer thickness is  
241 determined by the soil temperature profile by the end of the spinup in a no ice case, which is the  
242 simulation by the original CLM5 model without excess ice incorporated. Non-permafrost regions in the  
243 CAPS data are assigned the no ice landunit for 100% of their area. We emphasize that the prescribed  
244 cryostratigraphies are a first-order approximation that can by no means represent the wide variety of true  
245 ground ice conditions found in the permafrost domain. Nevertheless, this makes it possible to gauge the  
246 effect of excess ice melt on future projections of the permafrost thermal regime, when compared to  
247 “traditional” reference simulations without excess ice.

248 We design a tiling scheme prescribing the assignment of landunits for each CAPS class based on  
249 previous observations and empirical estimates (Table 2). All CAPS classes in this study are categorized  
250 into three levels of volumetric ice content (5%, 15%, and 25%) that are converted from the ranges (<10%,  
251 10-20%, and >20%) in the original CAPS data. The goal of our tiling scheme is to determine a  
252 combination of area weights of three excess ice landunits for each CAPS class, making the spatially  
253 averaged volumetric content of excess ice the same as that for the CAPS class. We assume that all CAPS  
254 classes have the same area fraction (20%) of the low ice landunit, and the CAPS classes with a higher  
255 ice content are due to the existence of the landunits with a higher content excess ice. We make this  
256 assumption based on previous studies that the segregated ice is widely distributed in permafrost.  
257 Observational studies have found segregated ice bodies in various continuous permafrost regions across  
258 the circum-arctic including West Central Alaska (Kanevskiy et al., 2014), Nunavik, Canada (Calmels  
259 and Allard, 2008), and Svalbard (Cable et al., 2018). In discontinuous permafrost regions, segregated ice  
260 bodies also commonly exist underneath Palsas and Lithasas, including Fennoscandia (Seppälä, 2011),  
261 Altai and Sayan, Russia (Iwanhana et al., 2012), Himalayas (Wünnemann et al., 2008), and Mongolia  
262 (Sharkhuu et al., 1999). The volumetric content of visible segregated ice bodies mentioned above ranges  
263 widely from 10-50% (Gilbert et al., 2016).

264 Given the tiling scheme prescribed above, all CAPS classes are assigned a 20% area of low ice  
265 landunit. Correspondingly, the CAPS classes with 15% volumetric ice content are assigned another 14%  
266 area weight for mid ice landunit on top of the CAPS classes with 5% volumetric ice content, while the  
267 CAPS classes with 25% volumetric ice are assigned another 22% area for high ice landunit on top of the  
268 CAPS classes with 15% volumetric ice content. The classes of “chf” and “chr” are the exceptions as their  
269 corresponding regions are typically with the landscape of Yedoma ~~and/or~~ ice wedge polygonal tundra  
270 ~~or both~~ (Kanevskiy et al., 2011; Gross et al., 2013). We therefore assign only the low and high ice  
271 landunits for these two CAPS classes. Summing up the landunit fractions for all the CAPS grid cells  
272 within each CLM grid cell obtains the area weights on the grid level that are stored in the surface data  
273 file. Figure 3 shows a schematic plot for the initialization scenario and the area covered by different

274 excess ice landunits as the result of sub-grid excess ice initialization in the global simulation case. Note  
275 that excess ice for some regions (e.g. Southern Norway and the Alps) can completely melt out during the  
276 spinup period since the CLM initial condition prescribes overly warm (non-permafrost) soil temperature  
277 for these regions.

278 In this study, we define the grid cells or landunits with permafrost as the ones having at least one  
279 hydrologically active soil layer that has been frozen in the last consecutive 24 months. In this case, we  
280 define permafrost degradation fully degraded permafrost when all landunits in one grid point are with cell  
281 have an active layer thickness of more than 6.5 metres, recognizing that in reality permafrost at many  
282 localities may continue to exist at greater depths. We also prepare a “grid-average ice case” by applying  
283 the same total amount of excess ice as in the sub-grid ice case in each soil layer, but using only one  
284 landunit instead of three that account for the sub-grid variability of excess ice. The volumetric content of  
285 excess ice in the single landunit is calculated as the spatial average of those in the three landunits in the  
286 triple-landunit case. This grid-average ice case provides a reference to evaluate the effects of the sub-  
287 grid excess ice representation on the global scale. Finally, we simulate a reference case without excess  
288 ice, denoted the “no ice case” in the following. Details on the three cases for the global simulations are  
289 listed in Table 3. All global cases are forced by the 3<sup>rd</sup> version of Global Soil Wetness Project forcing  
290 data (GSWP3; Kim et al., 2012), running in the Satellite Phenology (SP) mode. The International Land  
291 Atmosphere Model Benchmarking (ILAMB; Collier et al., 2018) project has indicated the superior  
292 performance of GSWP3 data forcing the CLM5 in the SP-only mode  
293 ([http://webext.cgd.ucar.edu/I20TR/\\_build\\_090817\\_CLM50SPONLY\\_CRUNCEP\\_GSWP3\\_WFDEI/in](http://webext.cgd.ucar.edu/I20TR/_build_090817_CLM50SPONLY_CRUNCEP_GSWP3_WFDEI/index.html)  
294 [dex.html](http://webext.cgd.ucar.edu/I20TR/_build_090817_CLM50SPONLY_CRUNCEP_GSWP3_WFDEI/index.html)). We conducted a 100-year spin-up using the 1901-1920 climatology before conducting  
295 historical period simulations covering 1901-2005. The anomaly forcing under the RCP8.5 scenario on  
296 top of the 1982-2005 climatology forces simulations in the projected period.

### 297 3. Result

#### 298 3.1 Excess ice melt simulations for Lena River delta cryostratigraphies

299 By the end of the spinup in the triple-landunit case, the active layer thickness is 0.85 m, 0.55 m, and  
300 0.45 m for the ice-poor terrain, the Holocene ice wedge terrain, and the Yedoma ice complex, respectively.  
301 On the other hand, the active layer thickness for the average ice single-landunit case is 0.85 m, which is  
302 the same as in the no excess ice terrain in the triple-landunit case. For the average ice single-landunit  
303 case, a small amount of excess ice ( $24\text{kg } \mu\text{m}^2\text{m}^{-2}$ ) melts during the spinup period, resulting in 2.6 cm  
304 surface subsidence throughout the grid.

305 For the Yedoma ice complex, very little excess ice melt in the 1950s, and it stabilizes afterwards  
306 until the late 2000s when substantial ice melt and surface subsidence starts to happen occur. For the  
307 Holocene ground ice terrain, there is no excess ice melt before the late 2010s. By the year 2100, the  
308 Yedoma ice complex has exhibited nearly 4 metres of surface subsidence, while the Holocene ground  
309 ice terrain has about 0.6 metres of surface subsidence (Figure 4). For the average ice single-landunit  
310 case, the noticeable excess ice melt and surface subsidence starts in the late 2010s, which creates about

311 0.5 meters of surface subsidence by 2100. The magnitude of surface subsidence in the average ice  
312 single-landunit case is lower than both the Holocene ground ice terrain and the Yedoma ice complex in  
313 the triple-landunit case.

314 On the grid scale, the total excess ice melt is higher in the average ice single-landunit case than in  
315 the triple-landunit case (Figure 5). By the year 2100, the average ice single-landunit case has about 30  
316  $\text{kg m}^{-2}\text{-m}^{-2}$  more excess ice melt than the triple-landunit case. The difference in excess ice on the grid  
317 level results from the different volumetric content of excess ice caused by the spatial averaging. In this  
318 way, the sub-grid representation of excess ice can potentially also provide more detailed and realistic  
319 representation of model variables on the grid level. This is particularly important for the CLM5, which  
320 serves as the land component in Earth System Models, which requires the coupling between interacting  
321 components on the grid level.

322 Compared to Westermann et al. (2016), the CLM5 with sub-grid excess ice simulates slightly less  
323 (~20% less) surface subsidence by 2100 for both the central delta and ice complex. We consider this a  
324 good agreement as we do not expect a closer fit of the model results due to substantial differences in the  
325 model physics (for example, the Cryogrid3 simulations in Westermann et al. (2016) lack a representation  
326 of the subsurface water cycle). What is in common between these two studies is the earlier start of excess  
327 ice melt and more surface subsidence in the ice complex than in the central delta. The CLM5 with sub-  
328 grid excess ice also exhibits the varying active layer thickness with different excess ice conditions as  
329 Cryogrid3 does. These results suggest that the new model development enables small-scale variability in  
330 excess ice melt and subsequent impacts in agreement with previously published modeling efforts.

### 331 3.2 Global projection of permafrost thaw and excess ice melt

332 Single-point simulations have shown that the varying excess ice cryostratigraphies for different  
333 landunits result in sub-grid variabilities of excess ice melt and surface subsidence under the warming  
334 climate. The same features remain in the sub-grid ice case within the global simulations that excess ice  
335 in the low ice landunit can completely melt out throughout the circum-Arctic permafrost region by the  
336 end of the 21<sup>st</sup> century (Figure 6). The modeled magnitude of surface subsidence is similar to the ~10 cm  
337 surface subsidence observed in Barrow and West Dock in the early 21st century (Shiklomanov et al.,  
338 2013; Streleskiy et al., 2017). The magnitude of surface subsidence is also comparable to the 1-4 cm  
339 decade<sup>-1</sup> surface subsidence rate on average over the North Slope of Alaska observed by satellite  
340 measurements since the 1990s (Liu et al., 2010). In comparison, the absence of surface subsidence for  
341 Arctic Alaska modeled by Lee et al. (2014) is due to an overly deep (1 m deep) excess ice initialization  
342 depth. By the year 2100, most ice in the medium ice landunit melts away in the sub-arctic region, while  
343 there is less ice melt in the colder regions such as the North Slope of Alaska and the central Siberia. The  
344 high ice landunit has the greatest surface subsidence among the three because of its high excess ice  
345 content, leading to 2-5 meters of surface subsidence by the year 2100.

346 The existence of excess ice modulates the thermal regime of permafrost soil and is a major control  
347 on permafrost degradation trajectories in a warming climate. Permafrost with excess ice consistently  
348 exhibits delayed permafrost degradation compared to the no ice case (Figure 7). For the no ice case

349 modeled by the original CLM5, more than half of the permafrost area undergoes degradation by the end  
350 of the 21<sup>st</sup> century. By 2100, the only areas where permafrost remains are the North Slope of Alaska,  
351 Northern Canada, and the majority of the land area in Northern Siberia. The areas with remaining  
352 permafrost in the year 2100 under the RCP8.5 scenarios are substantially larger compared to the CLM4  
353 simulations, in which nearly all permafrost in Eurasia becomes degraded (Lawrence et al., 2012). For the  
354 grid-average ice case, the presence of excess ice stabilizes the permafrost thermal regime and thus  
355 sustains a larger permafrost area on a global scale in the simulation. For example, permafrost areas in  
356 some subarctic regions in the eastern and western Siberia, as well as part of the Arctic coastal regions in  
357 Yukon Territory, Canada, remain in the grid-average ice case by 2100. Compared to the grid-average ice  
358 case, even more permafrost areas are sustained in the sub-grid ice case, most of which are located in  
359 southern Siberia. In the subarctic regions in Alaska and Northwest Canada as well as part of the central  
360 Siberia, permafrost degradation is delayed from the 2040s in the grid ice case to the 2080s in the sub-  
361 grid ice case. We emphasize that permafrost is only sustained according to the accepted temperature-  
362 based definition (ground material at temperature below zero for two consecutive years), but excess ice  
363 continuously melts in this process, which energetically is a different mode of permafrost degradation,  
364 similar to a negative mass balance of glaciers and ice sheets.

365 In the sub-grid ice case, the landunits with high excess ice contents lead to more grid points-cells  
366 for which permafrost conditions remain in the year 2100 compared to the grid-average ice case. On the  
367 other hand, permafrost with excess ice only covers a fraction of a grid pointcell. Among the permafrost  
368 degradation trajectories in the three global simulation cases (Figure 8), the sub-grid ice case can provide  
369 a more detailed picture on the timing of permafrost degradation. Grid cells become ‘partially degraded  
370 permafrost’ if landunits with excess ice still contain permafrost, which phenomenologically is a more  
371 realistic representation that also makes it possible to represent the permafrost distribution in the  
372 discontinuous and sporadic permafrost zones. On the other hand, only “fully degraded permafrost” and  
373 “remaining permafrost” can be distinguished for the no ice and grid-average ice case. Under the warming  
374 climate in the 21<sup>st</sup> century, the existence of excess ice, especially the high content of excess ice, has a  
375 stabilizing effect on soil temperature that delay the disappearance of permafrost on the sub-grid level.  
376 Therefore, by the year 2100, there are regions with partially degraded permafrost in between intact and  
377 degraded permafrost (Figure 8). For example, in western Siberia, the Pacific coastal area of eastern  
378 Siberia, Northwestern Canada, and along the Brooks Range in Alaska, taliks form for landunits with low  
379 excess ice contents which leads to partially degraded permafrost regions. Therefore, permafrost  
380 degradation exhibits a gradual transition from continuous to discontinuous permafrost, and to non-  
381 permafrost regions. Some of these regions also encounter substantial surface subsidence in the high ice  
382 landunit (> 5 m) (Figure 6).

383 We further compare the total permafrost area (defined as landunits with active layer thickness < 6.5  
384 metreers) in the three cases throughout time. The differences in permafrost area increase from the grid-  
385 average ice case and sub-grid ice case to the no ice case at a rate of 1000 km<sup>2</sup> per year until 2050 (Figure  
386 9). After 2050, the area difference of permafrost in the grid-average ice case and no ice cases rapidly  
387 increases, which reaches nearly one million km<sup>2</sup> by 2100. In the sub-grid ice case, the rate of increase

388 remains relatively unchanged after 2050, resulting in an about 0.2 million km<sup>2</sup> larger permafrost area  
389 than that in the no ice case.

#### 390 4. Discussion

391 The aim of the sub-grid excess ice representation in the CLM5 is to facilitate long-term global  
392 projection of excess ice melt and surface subsidence in the permafrost regions. Results from idealized  
393 sensitivity experiments (see supplemental material) implies that overly low volumetric content of excess  
394 ice, such as the grid-average ice case in this study and that in Lee et al. (2014), result in overly early start  
395 of excess ice melt and an overly high melting rate. It is because the higher content of excess ice covering  
396 a smaller area takes longer to absorb enough latent heat of fusion from the atmosphere before it can start  
397 melting. A good model performance in this way relies not only on the updated sub-grid representation of  
398 excess ice in the global land model, but also on retrieving accurate initial conditions of excess ice  
399 distribution. However, ~~but~~ the corresponding observational data for ~~both~~ background excess ice  
400 conditions and model evaluation is sparse, considering especially that drastic excess ice melt as modeled  
401 until 2100 is only observed in few locations today (e.g. Günther et al., 2015). In the following, we discuss  
402 the challenges and limitations of the sub-grid excess ice framework, and how this sub-grid representation  
403 can potentially help the development of other CLM components.

404 Both single-point and global test simulations in this study have shown that excess ice melts under a  
405 warming climate is sensitive to its initialization depth. The active-layer-dependent excess ice  
406 initialization in this study in the global simulation (sub-grid excess ice case) yields excess ice melt and  
407 surface subsidence rates in the early 2000s that are comparable to observations. The lower depths of the  
408 assumed excess ice body control the termination of excess ice melt which at the same time determines  
409 the onset of talik formation in many permafrost areas. Due to the scarcity of observational data, it is  
410 unclear to what extent the cryostratigraphies assumed in our tiling scheme can reproduce the true vertical  
411 extent of excess ice bodies at least in a statistical sense. Even so, we manage to make the prescribed  
412 excess ice condition as close to the previous results as possible. Firstly, our tiling scheme on the large  
413 scale strictly follows the CAPS data (Brown et al., 2002) in terms of the volumetric excess ice content.  
414 Furthermore, statistics by Zhang et al. (2000) suggest the ranges of the vertical extent of ice-rich  
415 permafrost of 0-2 metreers and 2-4 metreers respectively for the CAPS classes with low (5%) and  
416 medium (15%) ice content. Comparatively, the vertical extents permafrost with excess ice prescribed by  
417 our tiling scheme are respectively 1.36 metreers and 3.78 metreers for the same CAPS classes, both of  
418 which lie within the ranges in Zhang et al. (2000). The vertical extent of ice-rich permafrost for the high  
419 ice landunit is much higher than that (4-6 metreers) in Zhang et al. (2000), but the unmelted part of the  
420 ice bodies does not strongly affect the overall rate of excess ice melt, although the remaining ice can  
421 slightly change soil temperature and moisture of the surrounding permafrost. We therefore imply that  
422 our high ice landunit initialization would not induce a strong bias in excess ice melt projection in the 21st  
423 century.

**Commented [LC2]:** We have added discussions on the model's sensitivity.

424 Due to the lack of excess ice datasets and observational evidence, ~~our projections of excess ice melt~~  
425 ~~and surface subsidence likely have biases that arise from the need to make empirical estimates and~~  
426 ~~simplifications for the excess ice initialization scenarios in the global simulation cases, involve empirical~~  
427 ~~estimates and simplifications, which could bring biases to the projection of excess ice melt and surface~~  
428 ~~subsidence. For example, as the CAPS data is mostly based on visible ice bodies (i.e., not pore ice)~~  
429 ~~(Heginbottom et al., 1995), we used the reported volumetric ground ice content in the CAPS data to~~  
430 ~~approximate the volumetric content of excess ice during model initialization. We apply the volumetric~~  
431 ~~content of ground ice in the CAPS data approximately as the volumetric content of excess ice during~~  
432 ~~initialization as the CAPS data is mostly based on visible ice bodies (Heginbottom et al., 1995), not to~~  
433 ~~mention further~~ the determination of volumetric contents of excess ice for three landunits also results  
434 from sparse observations and empirical estimates. The prescribed excess ice cryostratigraphies ignore  
435 ice morphology and the variation of volumetric content of excess ice with soil depth, regarding excess  
436 ice as homogeneous ~~within each assigned sub-grid ice content type (low, mid, or high) (Figure 3, upper~~  
437 ~~panel), “ice cubes”~~. For the high ice landunit, we simplify the cryostratigraphy initialization to Yedoma  
438 type ice, which prescribes overly thick excess ice bodies out of the Yedoma regions (Schurr et al., 2015).  
439 A deficiency in the current version of source code ~~prevents us from initializing~~ ~~disables us to initialize~~  
440 non-Yedoma wedged ice for the high ice landunit ~~where it occurs outside~~ ~~out~~ of the Yedoma region.  
441 Future versions of our model development will have more freedom in ~~the stratigraphic configuration of~~  
442 ~~excess ice~~ ~~excess ice stratigraphy configuration~~, which ~~will make~~ ~~makes~~ it possible to prescribe different  
443 cryostratigraphies of the same landunit (e.g. the high ice landunit) for different locations. ~~Furthermore,~~  
444 ~~excess ice stratigraphy~~. Because of the above shortcomings in the excess ice initialization, we do not  
445 expect the modeled excess ice melt in this study to be an adequate representation of reality ~~yet~~. ~~However,~~  
446 ~~direct ingestion of new or improved~~ ~~while improved~~ observational data sets of excess ice contents and  
447 cryostratigraphies ~~would likely~~ ~~could be directly ingested to yield~~ ~~improved~~ ~~more accurate~~ results.  
448 However, a spatially distributed global dataset with quantitative information on excess ice stratigraphies  
449 does not exist at present. We emphasize that for a better projection of excess ice melt, more observational  
450 data of excess ice distribution and surface subsidence is required to further evaluate and validate the new  
451 model implementation of excess ice. On the regional scale, Jorgenson et al. (2008) presented a permafrost  
452 map of total ground ice volume for the uppermost 5 met~~re~~s of permafrost based on both observations  
453 and estimates for Alaska. In addition, O’Neill et al. (2019) compiled permafrost maps for Northern  
454 Canada by paleogeographic modeling, mapping the abundances of three types of excess ice respectively.  
455 Further improvements of model results depend on additional observationally constrained datasets of  
456 excess ice conditions on the global scale.

457 The area weights of the excess ice landunits (Table 2) in the global simulation are obtained from the  
458 higher-resolution CAPS points located within a CLM grid cell. However, complex landscape  
459 development, such as thermokarst ponds, requires knowledge of the met~~re~~-scale distribution, for  
460 example the extent and geometry of individual ice wedges (Langer et al., 2016; Nitzbon et al., 2019),  
461 which cannot be represented with the still coarse-scale excess ice classes from the CAPS map. One  
462 possible solution to represent this could be to include another layer of sub-grid tiles below the CLM  
463 landunit level, where the individual tiles can interact laterally. This would allow for the representation of

464 small-scale permafrost features within a large-scale landunit with a given excess ice content. An example  
465 of how this could work is given by Aas et al. (2019) who simulated both polygonal tundra and peat  
466 plateaus with a two-tile interactive setup. This is also similar to the recent representation of hillslope  
467 hydrology by Swenson et al. (2019), where sub-grid tiles (on the column level in CLM) were used to  
468 represent different elements in a representative hillslope. In the future development of CLM, this could  
469 be part of a more generic tiling system where lateral heat and mass fluxes could be switched on and off  
470 to represent a wide range of land surface processes that are currently ignored or parameterized in LSMs.  
471 Fisher and Koven (2020) have discussed the challenges and opportunities in such an adaptive and generic  
472 tiling system. We would also advocate for enhancing current tiling schemes in such a direction, which  
473 could substantially improve the realism in the representation of permafrost landscapes in LSMs. However,  
474 the success of such a tiling approach will rely heavily on the availability of adequate observational data,  
475 further highlighting the need for observational efforts and close collaboration between field scientists  
476 and modelers.

477 The more detailed simulation of permafrost degradation trajectory with a sub-grid representation of  
478 excess ice also builds more potential on better modeling the permafrost-carbon feedback with  
479 biogeochemistry activated (CLM5BGC). Excess ice stabilizes the permafrost thermal regime, therefore  
480 alter the rate of carbon releasing from the permafrost (Shuur et al., 2008). Improved projections of  
481 permafrost warming could also enhance modeling of vegetation type changes (e.g. shrub expansion) that  
482 determines the nitrogen uptake to the atmosphere (Lorant and Goetz, 2012). On the other hand, the  
483 possibility to simulate surface subsidence and excess ice meltwater formation also opens the possibility  
484 of a more accurate representation of wetland formation. The increase in the area of wetland and soil  
485 moisture have an impact of the balance of CH<sub>4</sub> and CO<sub>2</sub> releasing from the permafrost as more organic  
486 matter could decompose in an anaerobic pathway (Lawrence et al., 2015; Treat et al., 2015). Compared  
487 to the parameterized inundated area simulation in the CLM5 (Ekici et al., 2019), a process-based wetland  
488 physics scheme together with the sub-grid representation of excess ice in this study would substantially  
489 contribute to the biogeochemical modeling over the circum-arctic area.

## 490 **5. Conclusion**

491 This study develops a sub-grid representation of excess ice in the CLM5 and examines the impacts  
492 of the existence and melting of excess ice in the sub-grid scale in a warming climate. Extra landunits  
493 duplicated from the natural vegetated landunit in the CLM sub-grid hierarchy make it possible to  
494 prescribe up to three different excess ice conditions in each grid ~~point-cell~~ with permafrost.

495 A test over the Lena river delta showcases that the sub-grid representation of excess ice can retrieve  
496 the sub-grid variability of annual thaw-freeze state and the excess ice melt ~~and~~ surface subsidence  
497 through time. On the other hand, initializing excess ice homogeneously throughout the grid cell produces  
498 a smaller stabilization effect of excess ice to the permafrost thermal regime and the local surface  
499 subsidence under a warming climate. With a tiling scheme ingesting a global data set of excess ice  
500 condition into the CLM surface data, our model development shows the capability of portraying more  
501 details on simulating permafrost degradation trajectories. As excess ice thermally stabilizes the

502 permafrost on the sub-grid scale, permafrost degrades with a trajectory from continuous permafrost to  
503 discontinuous permafrost, and finally to a permafrost-free area. The modeled global pattern of permafrost  
504 therefore exhibits regions of discontinuous permafrost as the transition zone between the continuous  
505 permafrost and degraded permafrost.

506 This study, for the first time, used an ESM to project excess ice melt and surface subsidence and  
507 permafrost degradation with sub-grid variability. The approach of duplicating tiles at the landunit level  
508 instead of the column level allows more freedom for further developments in this direction. Furthermore,  
509 the new CLM tiling hierarchy has much more potential than representing more accurate excess ice  
510 physics as examined in this study. The accuracies of predicted excess ice melt and surface subsidence  
511 trends are limited at present by the available global-scale dataset and studies on excess ground ice  
512 conditions, thus further advancement of the excess ice modeling will rely ~~Further advancing the excess~~  
513 ~~ice modeling relies on additional~~ new or improved observational studies ~~or~~ datasets of the excess ground  
514 ice conditions ~~on aat the~~ global scale. The model development in our study, therefore, lays the foundation  
515 for further advances focusing on excess ice modeling and other processes in the CLM framework that  
516 could benefit from an improved sub-grid representation.

517

#### 518 ~~Code/Data Availability~~ Source code and data availability

519 The original Community Land Model is available at <https://github.com/ESCOMP/ctsm>. The source code  
520 of model development in this study is available from the corresponding author upon request.

#### 521 **Author contributions**

522 L.C conducted model development work and wrote the initial draft with additional contributions from  
523 all authors. H.L, S.W, and K.S.A provided ideas and help during the process of model development. H.L  
524 provided the code of excess ice physics in the earlier version of CLM. L.C prepared all figures.

#### 525 **Acknowledgments**

526 This study is funded by the Research Council of Norway KLIMAFORSK program (PERMANOR;  
527 RCN#255331). K.S.A is supported by the Research Council of Norway EMERALD project  
528 (RCN#294948). We thank Sarah Chadburn for helpful comments and suggestions in preparing this  
529 manuscript.

530

#### 531 **Reference**

- 532 Aas, K. S., Martin, L., Nitzbon, J., Langer, M., Boike, J., Lee, H., Berntsen, T. K., and Westermann, S.:  
533 Thaw processes in ice-rich permafrost landscapes represented with laterally coupled tiles in a  
534 land surface model, *The Cryosphere*, 13, 591-609, 10.5194/tc-13-591-2019, 2019.
- 535 Brown, J., Ferrians Jr, O., Heginbottom, J., and Melnikov, E.: Circum-Arctic map of permafrost and  
536 ground-ice conditions, US Geological Survey Reston, VA, 1997.

537 Burke, E. J., Dankers, R., Jones, C. D., and Wiltshire, A. J.: A retrospective analysis of pan Arctic  
538 permafrost using the JULES land surface model, *Climate Dynamics*, 41, 1025-1038,  
539 10.1007/s00382-012-1648-x, 2013.

540 Cable, S., Elberling, B., and Kroon, A.: Holocene permafrost history and cryostratigraphy in the High-  
541 Arctic Adventdalen Valley, central Svalbard, *Boreas*, 47, 423-442, 10.1111/bor.12286, 2018.

542 Calmels, F., and Allard, M.: Segregated ice structures in various heaved permafrost landforms through  
543 CT Scan, *Earth Surface Processes and Landforms*, 33, 209-225, 10.1002/esp.1538, 2008.

544 Collier, N., Hoffman, F. M., Lawrence, D. M., Keppel-Aleks, G., Koven, C. D., Riley, W. J., Mu, M.,  
545 and Randerson, J. T.: The International Land Model Benchmarking (ILAMB) system: design,  
546 theory, and implementation, *Journal of Advances in Modeling Earth Systems*, 10, 2731-2754,  
547 2018.

548 Ekici, A., Lee, H., Lawrence, D. M., Swenson, S. C., and Prigent, C.: Ground subsidence effects on  
549 simulating dynamic high-latitude surface inundation under permafrost thaw using CLM5,  
550 *Geosci. Model Dev.*, 12, 5291-5300, 10.5194/gmd-12-5291-2019, 2019.

551 Fedorova, I., Chetverova, A., Bolshiyarov, D., Makarov, A., Boike, J., Heim, B., Morgenstern, A.,  
552 Overduin, P. P., Wegner, C., Kashina, V., Eulenburg, A., Dobrotina, E., and Sidorina, I.: Lena  
553 Delta hydrology and geochemistry: long-term hydrological data and recent field observations,  
554 *Biogeosciences*, 12, 345-363, 10.5194/bg-12-345-2015, 2015.

555 Fisher, R. A., and Koven, C. D.: Perspectives on the future of Land Surface Models and the challenges  
556 of representing complex terrestrial systems, *Journal of Advances in Modeling Earth Systems*,  
557 n/a, 10.1029/2018MS001453, 2020.

558 Fritz, M., Wetterich, S., Meyer, H., Schirrmeister, L., Lantuit, H., and Pollard, W. H.: Origin and  
559 characteristics of massive ground ice on Herschel Island (western Canadian Arctic) as revealed  
560 by stable water isotope and Hydrochemical signatures, *Permafrost and Periglacial Processes*, 22,  
561 26-38, 10.1002/ppp.714, 2011.

562 Gilbert, G. L., Kanevskiy, M., and Murton, J. B.: Recent Advances (2008–2015) in the Study of Ground  
563 Ice and Cryostratigraphy, *Permafrost and Periglacial Processes*, 27, 377-389, 10.1002/ppp.1912,  
564 2016.

565 Grosse, G., Romanovsky, V., Jorgenson, T., Anthony, K. W., Brown, J., and Overduin, P. P.:  
566 Vulnerability and feedbacks of permafrost to climate change, *Eos, Transactions American  
567 Geophysical Union*, 92, 73-74, 2011.

568 Grosse, G., Robinson, J. E., Bryant, R., Taylor, M. D., Harper, W., DeMasi, A., Kyker-Snowman, E.,  
569 Veremeeva, A., Schirrmeister, L., and Harden, J.: Distribution of late Pleistocene ice-rich  
570 syngenetic permafrost of the Yedoma Suite in east and central Siberia, Russia, *US Geological  
571 Survey Open File Report*, 2013, 1-37, 2013.

572 Günther, F., Overduin, P. P., Yakshina, I. A., Opel, T., Baranskaya, A. V., and Grigoriev, M. N.:  
573 Observing Muostakh disappear: permafrost thaw subsidence and erosion of a ground-ice-rich  
574 island in response to arctic summer warming and sea ice reduction, *The Cryosphere*, 9, 151-178,  
575 10.5194/tc-9-151-2015, 2015.

576 Heginbottom, J.A., Dubreuil, M.A. and Harker, P.A.: Canada, Permafrost. National Atlas of Canada.  
577 Natural Resources Canada, 5th Edition, MCR, 4177, 1995.

578 Hugelius, G., Strauss, J., Zubrzycki, S., Harden, J. W., Schuur, E. A. G., Ping, C. L., Schirmermeister, L.,  
579 Grosse, G., Michaelson, G. J., Koven, C. D., O'Donnell, J. A., Elberling, B., Mishra, U., Camill,  
580 P., Yu, Z., Palmtag, J., and Kuhry, P.: Estimated stocks of circumpolar permafrost carbon with  
581 quantified uncertainty ranges and identified data gaps, *Biogeosciences*, 11, 6573-6593,  
582 10.5194/bg-11-6573-2014, 2014.

583 Kanevskiy, M., Shur, Y., Fortier, D., Jorgenson, M. T., and Stephani, E.: Cryostratigraphy of late  
584 Pleistocene syngenetic permafrost (yedoma) in northern Alaska, Itkillik River exposure,  
585 *Quaternary Research*, 75, 584-596, 10.1016/j.yqres.2010.12.003, 2011.

586 Iwahana, G., Fukui, K., Mikhailov, N., Ostanin, O., and Fujii, Y.: Internal Structure of a Lithalsa in the  
587 Akkol Valley, Russian Altai Mountains, 23, 107-118, 10.1002/pp

588 Jorgenson, M., Yoshikawa, K., Kanevskiy, M., Shur, Y., Romanovsky, V., Marchenko, S., Grosse, G.,  
589 Brown, J., and Jones, B.: Permafrost characteristics of Alaska, *Proceedings of the Ninth*  
590 *International Conference on Permafrost*, 2008, 121-122.p.1734, 2012.

591 Kanevskiy, M., Jorgenson, T., Shur, Y., O'Donnell, J. A., Harden, J. W., Zhuang, Q., and Fortier, D.:  
592 Cryostratigraphy and Permafrost Evolution in the Lacustrine Lowlands of West-Central Alaska,  
593 *Permafrost and Periglacial Processes*, 25, 14-34, 10.1002/ppp.1800, 2014.

594 Kim, H., Yoshimura, K., Chang, E., Famiglietti, J., and Oki, T.: Century long observation constrained  
595 global dynamic downscaling and hydrologic implication, *AGU Fall Meeting Abstracts*, 2012.

596 Kokelj, S. V., Lacelle, D., Lantz, T. C., Tunnicliffe, J., Malone, L., Clark, I. D., and Chin, K. S.: Thawing  
597 of massive ground ice in mega slumps drives increases in stream sediment and solute flux across  
598 a range of watershed scales, *Journal of Geophysical Research: Earth Surface*, 118, 681-692,  
599 10.1002/jgrf.20063, 2013.

600 Koven, C. D., Ringeval, B., Friedlingstein, P., Ciais, P., Cadule, P., Khvorostyanov, D., Krinner, G., and  
601 Tarnocai, C.: Permafrost carbon-climate feedbacks accelerate global warming, *Proceedings of*  
602 *the National Academy of Sciences*, 108, 14769-14774, 2011.

603 Langer, M., Westermann, S., Boike, J., Kirillin, G., Grosse, G., Peng, S., and Krinner, G.: Rapid  
604 degradation of permafrost underneath waterbodies in tundra landscapes—toward a  
605 representation of thermokarst in land surface models, *Journal of Geophysical Research: Earth*  
606 *Surface*, 121, 2446-2470, 2016.

607 Langer, M., Westermann, S., Heikenfeld, M., Dorn, W., and Boike, J.: Satellite-based modeling of  
608 permafrost temperatures in a tundra lowland landscape, *Remote Sensing of Environment*, 135,  
609 12-24, <https://doi.org/10.1016/j.rse.2013.03.011>, 2013.

610 Lawrence, D. M., Slater, A. G., Romanovsky, V. E., and Nicolsky, D. J.: Sensitivity of a model projection  
611 of near-surface permafrost degradation to soil column depth and representation of soil organic  
612 matter, *Journal of Geophysical Research: Earth Surface*, 113, 10.1029/2007JF000883, 2008.

613 Lawrence, D. M., Oleson, K. W., Flanner, M. G., Thornton, P. E., Swenson, S. C., Lawrence, P. J., Zeng,  
614 X., Yang, Z. L., Levis, S., and Sakaguchi, K.: Parameterization improvements and functional  
615 and structural advances in version 4 of the Community Land Model, *Journal of Advances in  
616 Modeling Earth Systems*, 3, 2011.

617 Lawrence, D. M., Slater, A. G., and Swenson, S. C.: Simulation of present-day and future permafrost and  
618 seasonally frozen ground conditions in CCSM4, *Journal of Climate*, 25, 2207-2225, 2012.

619 Lawrence, D. M., Koven, C. D., Swenson, S. C., Riley, W. J., and Slater, A. G.: Permafrost thaw and  
620 resulting soil moisture changes regulate projected high-latitude CO<sub>2</sub> and CH<sub>4</sub> emissions,  
621 *Environmental Research Letters*, 10, 094011, 10.1088/1748-9326/10/9/094011, 2015.

622 Lawrence, D. M., Fisher, R. A., Koven, C. D., Oleson, K. W., Swenson, S. C., Bonan, G., Collier, N.,  
623 Ghimire, B., van Kampenhou, L., Kennedy, D., Kluzek, E., Lawrence, P. J., Li, F., Li, H.,  
624 Lombardozzi, D., Riley, W. J., Sacks, W. J., Shi, M., Vertenstein, M., Wieder, W. R., Xu, C.,  
625 Ali, A. A., Badger, A. M., Bisht, G., van den Broeke, M., Brunke, M. A., Burns, S. P., Buzan,  
626 J., Clark, M., Craig, A., Dahlin, K., Drewniak, B., Fisher, J. B., Flanner, M., Fox, A. M., Gentine,  
627 P., Hoffman, F., Keppel-Aleks, G., Knox, R., Kumar, S., Lenaerts, J., Leung, L. R., Lipscomb,  
628 W. H., Lu, Y., Pandey, A., Pelletier, J. D., Perket, J., Randerson, J. T., Ricciuto, D. M.,  
629 Sanderson, B. M., Slater, A., Subin, Z. M., Tang, J., Thomas, R. Q., Val Martin, M., and Zeng,  
630 X.: The Community Land Model Version 5: Description of New Features, Benchmarking, and  
631 Impact of Forcing Uncertainty, 11, 4245-4287, 10.1029/2018ms001583, 2019.

632 Lee, H., Swenson, S. C., Slater, A. G., and Lawrence, D. M.: Effects of excess ground ice on projections  
633 of permafrost in a warming climate, *Environmental Research Letters*, 9, 124006, 2014.

634 Liu, L., Zhang, T., and Wahr, J.: InSAR measurements of surface deformation over permafrost on the  
635 North Slope of Alaska, *Journal of Geophysical Research: Earth Surface*, 115,  
636 10.1029/2009jfr001547, 2010.

637 Loranty, M. M., and Goetz, S. J.: Shrub expansion and climate feedbacks in Arctic tundra, *Environmental  
638 Research Letters*, 7, 011005, 10.1088/1748-9326/7/1/011005, 2012.

639 Nitzbon, J., Langer, M., Westermann, S., Martin, L., Aas, K. S., and Boike, J.: Pathways of ice-wedge  
640 degradation in polygonal tundra under different hydrological conditions, *The Cryosphere*, 13,  
641 1089-1123, 10.5194/tc-13-1089-2019, 2019.

642 Nitzbon, J., Westermann, S., Langer, M., Martin, L. C. P., Strauss, J., Laboor, S., and Boike, J.: Fast  
643 response of cold ice-rich permafrost in northeast Siberia to a warming climate, *Nature*  
644 *Communications*, 11, 2201, 10.1038/s41467-020-15725-8, 2020.

645 O'Neill, H. B., Wolfe, S. A., and Duchesne, C.: New ground ice maps for Canada using a paleogeographic  
646 modelling approach, *The Cryosphere*, 13, 753-773, 10.5194/tc-13-753-2019, 2019.

647 Pascale, G. P. D., Pollard, W. H., and Williams, K. K. J. o. G. R. A.: Geophysical mapping of ground  
648 ice using a combination of capacitive coupled resistivity and ground-penetrating radar,  
649 *Northwest Territories, Canada*, 113, 2008.

650 Rachold, V., and Grigoriev, M.: Russian-German Cooperation SYSTEM LAPTEV SEA 2000: The Lena  
651 Delta 1998 Expedition, *Berichte zur Polarforschung (Reports on Polar Research)*, 315, 1999.

652 Schaefer, K., Lantuit, H., Romanovsky, V. E., Schuur, E. A. G., and Witt, R.: The impact of the  
653 permafrost carbon feedback on global climate, *Environmental Research Letters*, 9, 085003,  
654 10.1088/1748-9326/9/8/085003, 2014.

655 Schirrmeyer, L., Grosse, G., Schwamborn, G., Andreev, A. A., Meyer, H., Kunitsky, V. V., Kuznetsova,  
656 T. V., Dorozhkina, M. V., Pavlova, E. Y., Bobrov, A. A., and Oezen, D.: Late Quaternary  
657 History of the Accumulation Plain North of the Chekanovsky Ridge (Lena Delta, Russia): A  
658 Multidisciplinary Approach, *Polar Geography*, 27, 277-319, 10.1080/789610225, 2003.

659 Schirrmeyer, L., Grosse, G., Schnelle, M., Fuchs, M., Krbetschek, M., Ulrich, M., Kunitsky, V.,  
660 Grigoriev, M., Andreev, A., Kienast, F., Meyer, H., Babiy, O., Klimova, I., Bobrov, A.,  
661 Wetterich, S., and Schwamborn, G.: Late Quaternary paleoenvironmental records from the  
662 western Lena Delta, Arctic Siberia, *Palaeogeography, Palaeoclimatology, Palaeoecology*, 299,  
663 175-196, <https://doi.org/10.1016/j.palaeo.2010.10.045>, 2011.

664 Schirrmeyer, L., Froese, D., Tumskey, V., Grosse, G., and Wetterich, S.: Yedoma: Late Pleistocene ice-  
665 rich syngenetic permafrost of Beringia, in: *Encyclopedia of Quaternary Science*. 2nd edition,  
666 Elsevier, 542-552, 2013.

667 Schneider, J., Grosse, G., and Wagner, D.: Land cover classification of tundra environments in the Arctic  
668 Lena Delta based on Landsat 7 ETM+ data and its application for upscaling of methane  
669 emissions, *Remote Sensing of Environment*, 113, 380-391,  
670 <https://doi.org/10.1016/j.rse.2008.10.013>, 2009.

671 Schuur, E. A., Bockheim, J., Canadell, J. G., Euskirchen, E., Field, C. B., Goryachkin, S. V., Hagemann,  
672 S., Kuhry, P., Lafleur, P. M., and Lee, H.: Vulnerability of permafrost carbon to climate change:  
673 Implications for the global carbon cycle, *BioScience*, 58, 701-714, 2008.

674 Schuur, E. A. G., McGuire, A. D., Schädel, C., Grosse, G., Harden, J. W., Hayes, D. J., Hugelius, G.,  
675 Koven, C. D., Kuhry, P., Lawrence, D. M., Natali, S. M., Olefeldt, D., Romanovsky, V. E.,  
676 Schaefer, K., Turetsky, M. R., Treat, C. C., and Vonk, J. E.: Climate change and the permafrost  
677 carbon feedback, *Nature*, 520, 171, 10.1038/nature14338, 2015.

678 Schwamborn, G., Rachold, V., and Grigoriev, M. N.: Late Quaternary sedimentation history of the Lena  
679 Delta, *Quaternary International*, 89, 119-134, [https://doi.org/10.1016/S1040-6182\(01\)00084-2](https://doi.org/10.1016/S1040-6182(01)00084-2),  
680 2002.

681 Seppälä, M.: Synthesis of studies of palsa formation underlining the importance of local environmental  
682 and physical characteristics, *Quaternary Research*, 75, 366-370,  
683 <https://doi.org/10.1016/j.yqres.2010.09.007>, 2011.

684 Sharkhuu, N.: Occurrence of frost heaving in the Selenge River Basin, Mongolia, 10, 187-192,  
685 10.1002/(sici)1099-1530(199904/06)10:2<187::Aid-ppp294>3.0.Co;2-w, 1999.

686 Shiklomanov, N. I., Streletskiy, D. A., Little, J. D., and Nelson, F. E.: Isotropic thaw subsidence in  
687 undisturbed permafrost landscapes, *Geophysical Research Letters*, 40, 6356-6361,  
688 10.1002/2013gl058295, 2013.

689 Slater, A. G., and Lawrence, D. M.: Diagnosing present and future permafrost from climate models,  
690 *Journal of Climate*, 26, 5608-5623, 2013.

691 Streletskiy, D. A., Shiklomanov, N. I., Little, J. D., Nelson, F. E., Brown, J., Nyland, K. E., and Klene,  
692 A. E.: Thaw Subsidence in Undisturbed Tundra Landscapes, Barrow, Alaska, 1962–2015,  
693 *Permafrost and Periglacial Processes*, 28, 566-572, 10.1002/ppp.1918, 2017.

694 Swenson, S. C., Clark, M., Fan, Y., Lawrence, D. M., and Perket, J.: Representing Intrahillslope Lateral  
695 Subsurface Flow in the Community Land Model, *Journal of Advances in Modeling Earth  
696 Systems*, 11, 4044-4065, 10.1029/2019MS001833, 2019.

697 Treat, C. C., Natali, S. M., Emakovich, J., Iversen, C. M., Lupascu, M., McGuire, A. D., Norby, R. J.,  
698 Roy Chowdhury, T., Richter, A., Šantrůčková, H., Schädel, C., Schuur, E. A. G., Sloan, V. L.,  
699 Turetsky, M. R., and Waldrop, M. P.: A pan-Arctic synthesis of CH<sub>4</sub> and CO<sub>2</sub> production from  
700 anoxic soil incubations, 21, 2787-2803, 10.1111/gcb.12875, 2015.

701 Turetsky, M. R., Abbott, B. W., Jones, M. C., Anthony, K. W., Olefeldt, D., Schuur, E. A., Koven, C.,  
702 McGuire, A. D., Grosse, G., and Kuhry, P.: Permafrost collapse is accelerating carbon release,  
703 *Nature*, 569, 32-34, 2019.

704 Ulrich, M., Grosse, G., Chabrillat, S., and Schirmermeister, L.: Spectral characterization of periglacial  
705 surfaces and geomorphological units in the Arctic Lena Delta using field spectrometry and  
706 remote sensing, *Remote Sensing of Environment*, 113, 1220-1235,  
707 <https://doi.org/10.1016/j.rse.2009.02.009>, 2009.

708 Walter, K. M., Zimov, S. A., Chanton, J. P., Verbyla, D., and Chapin, F. S.: Methane bubbling from  
709 Siberian thaw lakes as a positive feedback to climate warming, *Nature*, 443, 71-75,  
710 10.1038/nature05040, 2006.

711 West, J. J., and Plug, L. J.: Time-dependent morphology of thaw lakes and taliks in deep and shallow  
712 ground ice, *Journal of Geophysical Research: Earth Surface*, 113, 10.1029/2006jf000696, 2008.

713 Westermann, S., Langer, M., Boike, J., Heikenfeld, M., Peter, M., Eitzelmüller, B., and Krinner, G.:  
714 Simulating the thermal regime and thaw processes of ice-rich permafrost ground with the land-  
715 surface model CryoGrid 3, *Geosci. Model Dev.*, 9, 523-546, 10.5194/gmd-9-523-2016, 2016.

716 Wünnemann, B., Reinhardt, C., Kotlia, B. S., and Riedel, F.: Observations on the relationship between  
717 lake formation, permafrost activity and lithalsa development during the last 20 000 years in the  
718 Tso Kar basin, Ladakh, India, 19, 341-358, 10.1002/ppp.631, 2008.

719 Zhang, T., Barry, R. G., Knowles, K., Heginbottom, J. A., and Brown, J.: Statistics and characteristics  
720 of permafrost and ground-ice distribution in the Northern Hemisphere, *Polar Geography*, 23,  
721 132-154, 10.1080/10889379909377670, 1999.

722 Zhang, T., Heginbottom, J. A., Barry, R. G., and Brown, J.: Further statistics on the distribution of  
723 permafrost and ground ice in the Northern Hemisphere, *Polar Geography*, 24, 126-131,  
724 10.1080/10889370009377692, 2000.

725 Zimov, S. A., Schuur, E. A., and Chapin, F. S.: Permafrost and the global carbon budget, *Science*, 312,  
726 1612-1613, 2006.

727

728 **Table 1: The excess ice initialization scenario in each of the three terraces (landunits) for the Lena**  
 729 **River delta, as well as that for the single-landunit excess ice initialization case.**  
 730

Depth (after adding ice)	Volumetric Ice content	Area weight
No excess ice terrain		
N/A	0%	24.6%
Holocene ground ice terrain		
0.9-9 m	65%	66.6%
Yedoma ice complex		
0.6-20 m	90%	8.8%
Average ice single-landunit case		
0.6-0.9 m	7.92%	100%
0.9-9 m	51.21%	100%
9-20 m	7.92%	100%

731

732

733 **Table 2: The tiling scheme prescribing area weights of landunits for each CAPS class. The detailed**  
 734 **CAPS classes are shown in Figure 2.**

Overall visible ground ice content for each CAPS point	Tiling scheme (area weights for each excess ice category)	Eligible CAPS types
5%	80% no excess ice; 20% Low	clf; clf; slf; ilf; clr; dlr; slr; ilr
15%	58% no excess ice; 20% Low; 22% Medium	cmf; dmf; smf; imf; dhr; shr; ihr
15%	66% no excess ice; 20% Low; 14% High	chr
25%	44% no excess ice; 20% Low; 22% Medium; 14% High	dhf; shf; ihf
25%	52% no excess ice; 20% Low; 28% High	chf

735 Note: For each class, the first letter is for the permafrost extent, the second for the excess ice content, and the third  
 736 for the terrain and overburden, following Brown et al. (2002).

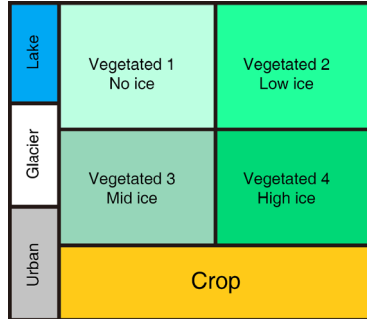
737

738 **Table 3: List of simulations conducted for this study.**

Cases	Description
Single point cases for the Lena river delta	
Triple-landunit case	Applying the sub-grid representation of excess ice. Three natural vegetated landunit initialized.
Average ice single-landunit case	Not applying the sub-grid representation of excess ice. Only one natural vegetated landunit initialized. The grid-mean excess ice content for each soil layer in the only landunit is calculated by spatially averaging those in different landunits in the triple-landunit case.
Global simulation cases	
No ice case	Not adding any excess ground ice (the original CLM5 simulation).
Sub-grid ice case	Applying the sub-grid representation of excess ice. A tiling scheme helps to “translate” excess ice conditions in the CAPS data to fit what the CLM5 requires.
Grid-average ice case	Not applying the sub-grid representation of excess ice. The grid-mean excess ice content for each soil layer is calculated by spatially averaging those in different landunits in the sub-grid ice case.

739

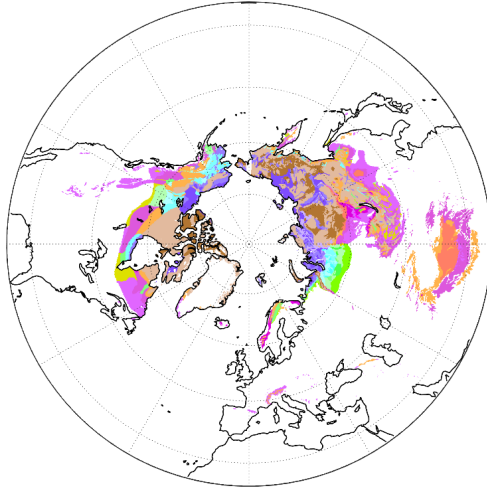
740



741

742 **Figure 1: Modification of the CLM5 tiling hierarchy on the landunit level containing four natural**  
 743 **vegetated landunits for different excess ice conditions.**

744



**Permafrost area classification**

Permafrost Extent	Ground Ice Content (percent by volume)					
	Lowlands, highlands, and intra-and intermontane depressions			Mountains, highlands, ridges, and plateaus		
	25%	15%	5%	15%	5%	
Continuous (100%)	chf	cmf	clf	chr	clr	
Discontinuous (70%)	dhf	dmf	dlf	dhr	dhr	dtr
Sporadic (30%)	shf	smf	slf	shr	str	
Isolated (5%)	ihf	imf	ilf	ihr	itr	

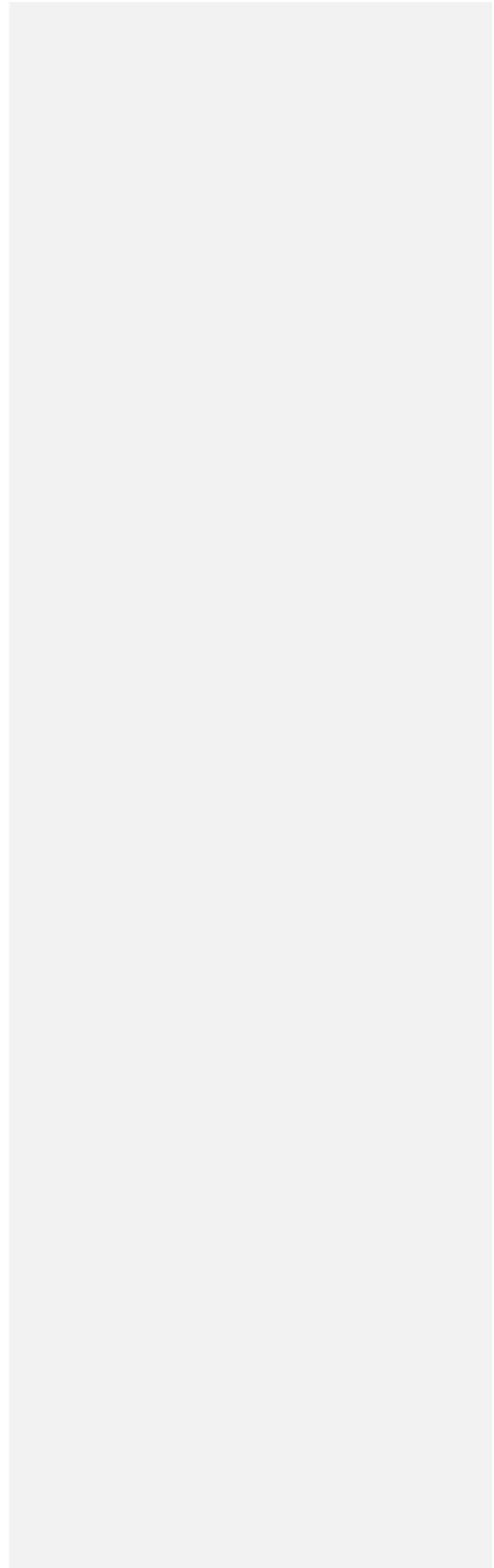
\* Letter code naming: The first letter is for the permafrost extent, second for the ground excess ice content, and the third for the terrain and overburden.

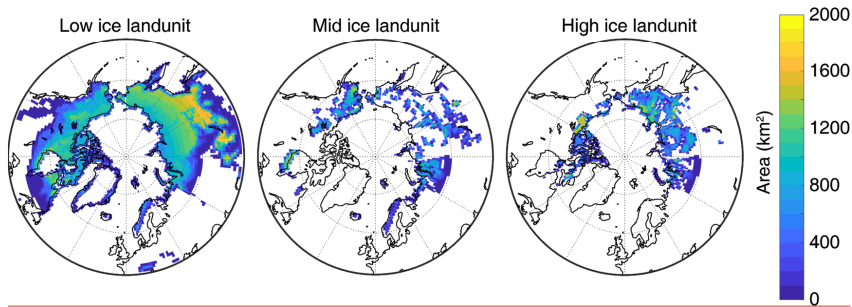
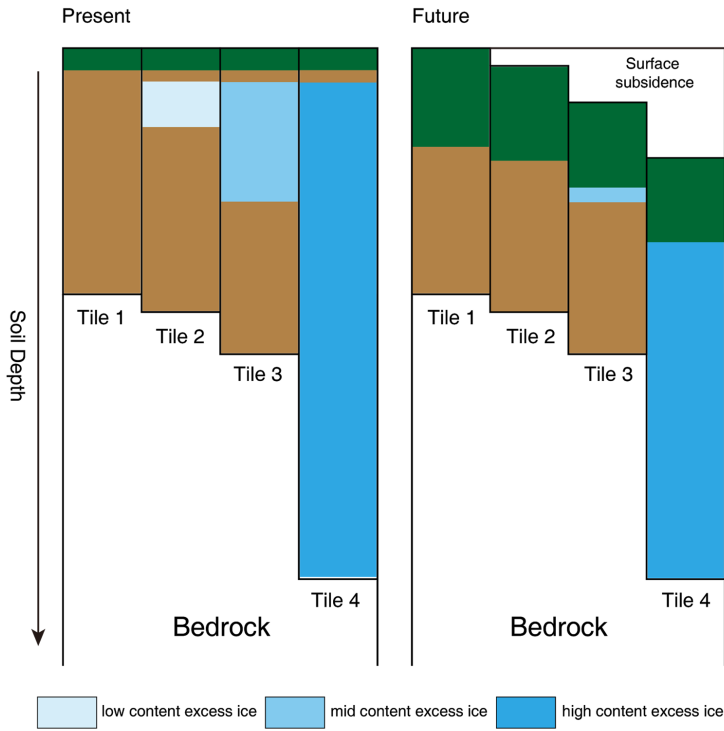
745

746 **Figure 2: Spatial distribution of excess ground ice in the Northern Hemisphere modified from**  
 747 **Brown et al. (2002). Compared to the original data, permafrost extents and ground ice contents**  
 748 **are converted to definite numbers (percentages) for model computation.**

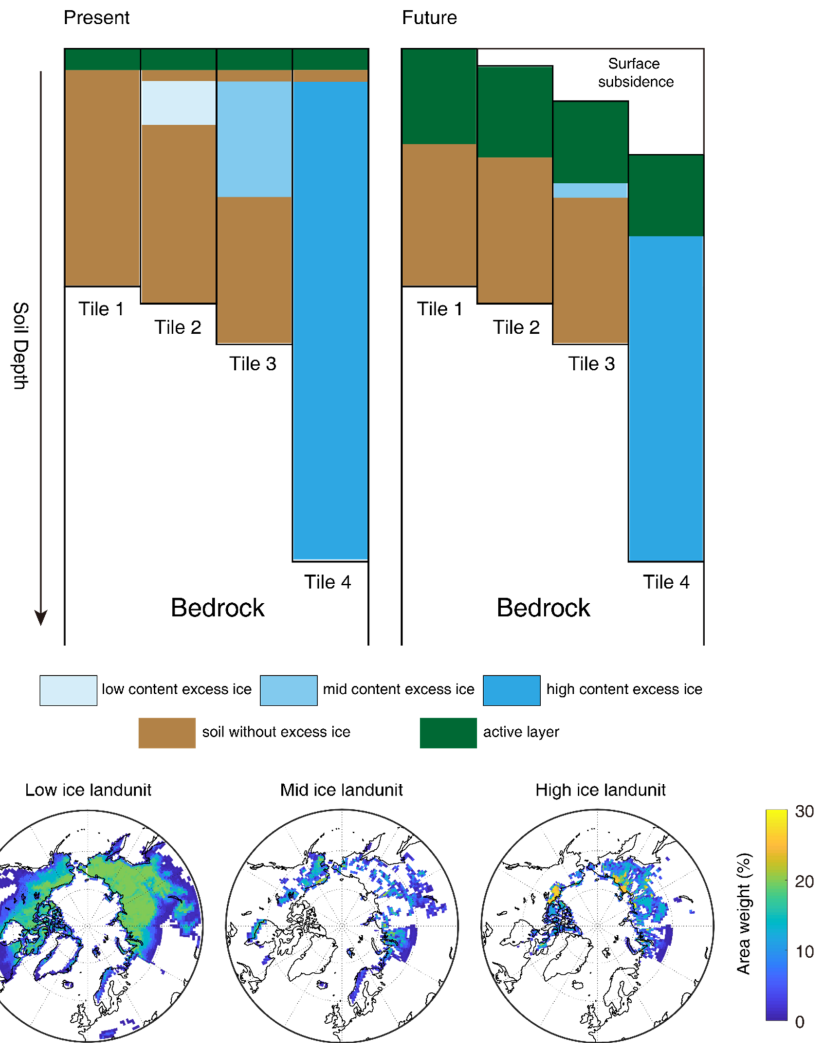
749

750





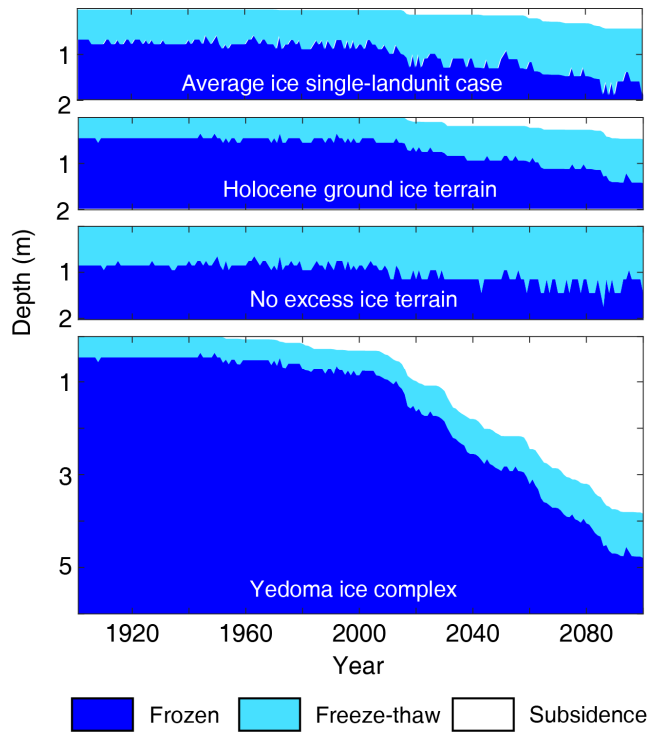
751



752

753 Figure 3. Schematic representation of the sub-grid excess ice initialization scenario, and maps  
 754 showing the area **weight (%)** occupied by different excess ice landunits, i.e. the initial condition of  
 755 excess ice in the global simulation.

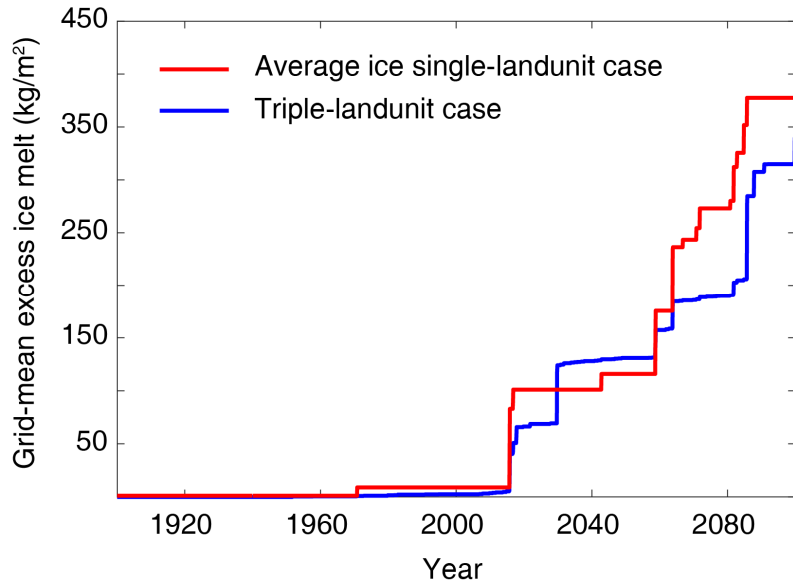
756



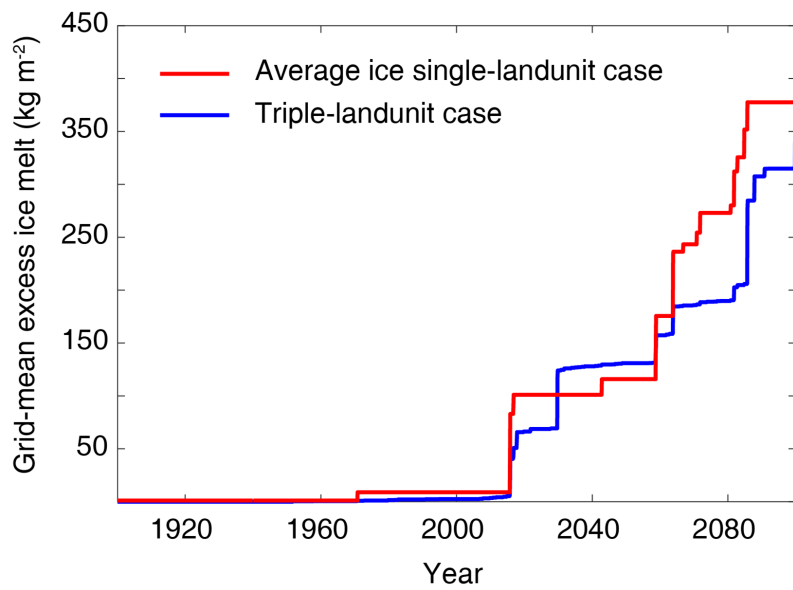
757

758 **Figure 4.** Annual freeze-thaw state for the three terraces for the triple-landunit case, as well as for  
 759 the average ice single-landunit case.

760



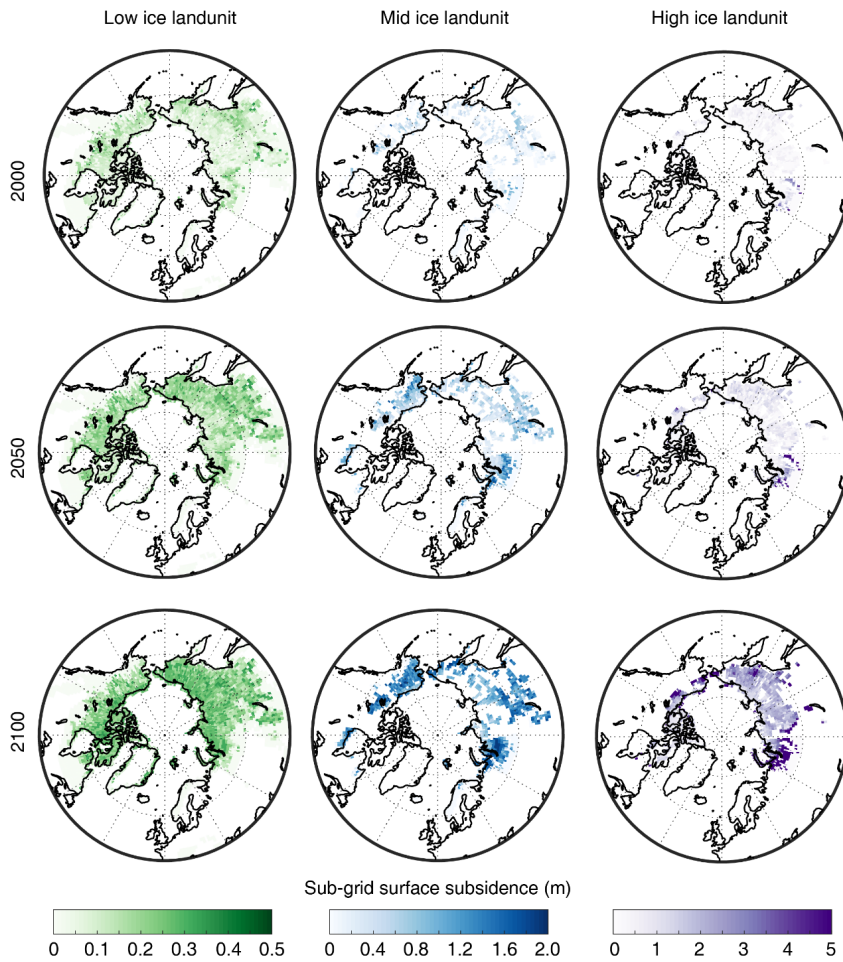
761



762

763 Figure 5. Grid-mean excess ice melt since 1900 for the single-point cases over the Lena river delta  
 764 with and without the sub-grid excess ice initialization.

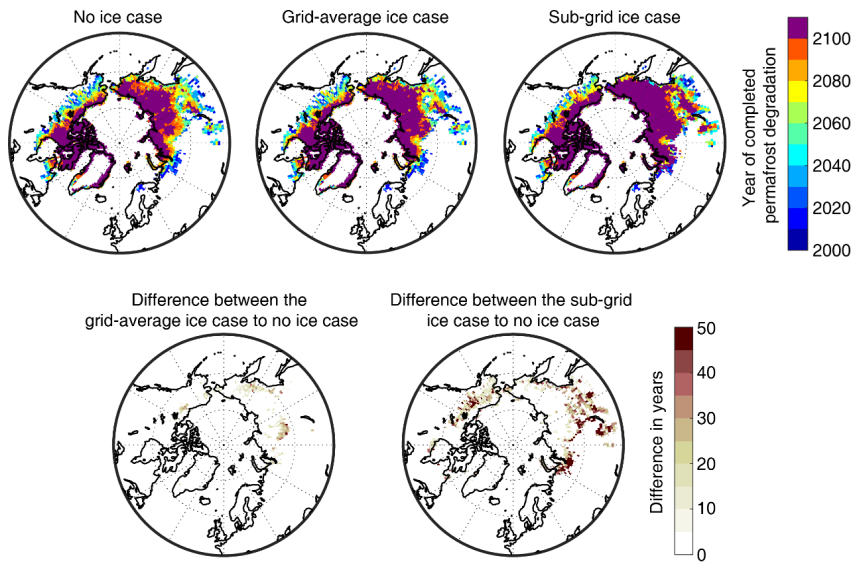
765



766

767 **Figure 6. Maps showing sub-grid surface subsidence (m) in 2000, 2050, 2100 in the low, mid, and**  
 768 **high excess ice landunits in the sub-grid ice case.**

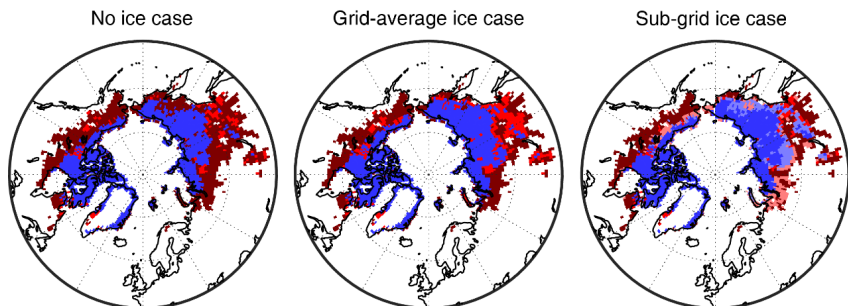
769



770

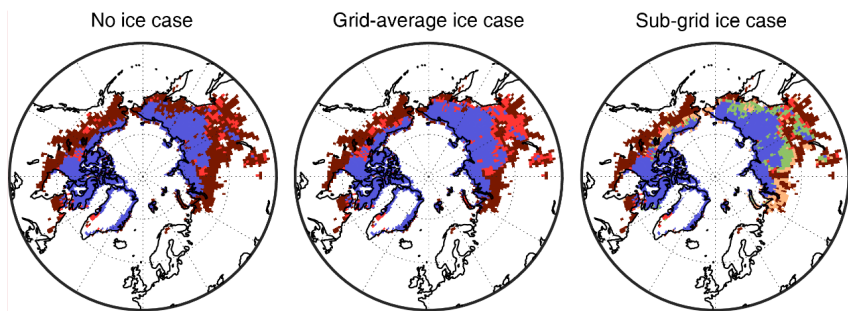
771 **Figure 7. Maps showing the year of completed permafrost degradation (upper set of three maps),**  
 772 **as well as the differences between cases (lower set of two maps). The purple color indicates the**  
 773 **existence of permafrost in these grid points-cells by 2100. The difference in years is provided only**  
 774 **for grid cell with completed permafrost degradation before 2100.**

775



776

- Remaining permafrost      ■ Partially degraded permafrost, without talik
- Partially degraded permafrost, with talik      ■ Fully degraded permafrost, without year-round unfrozen soil
- Fully degraded permafrost, with year-round unfrozen soil



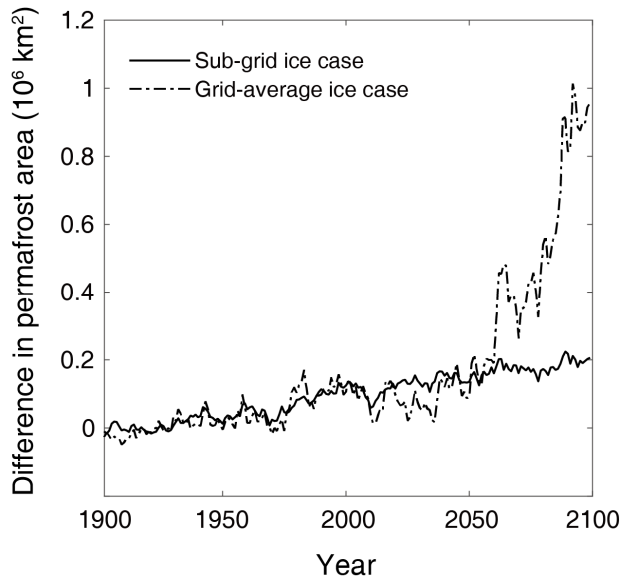
777

- Remaining permafrost      ■ Partially degraded permafrost, without talik
- Partially degraded permafrost, with talik      ■ Fully degraded permafrost, without year-round unfrozen soil
- Fully degraded permafrost, with year-round unfrozen soil

Commented [LC3]: We have changed the colors to make them more distinct.

778 **Figure 8. Maps of different stages of permafrost degradation diagnosed from the model output by**  
 779 **the year 2100. “Year-round unfrozen soil” in the fully degraded permafrost region is defined as the**  
 780 **part of degraded permafrost in which the soil temperature never decrease below 0 °C in any time**  
 781 **of year, which is in the same manner as talik in the permafrost area.**

782



783

784 Figure 9. Difference in modeled permafrost area vs. versus time between the sub-grid ice case and  
 785 no ice case, as well as between the grid-average ice case and no ice case.

786

## Supplemental material for Projecting Circum-Arctic Excess Ground Ice Melt with a sub-grid representation in the Community Land Model

### S1. The sensitivity of excess ice melt and corresponding impacts to its sub-grid distribution

We design idealized single-grid simulation cases, aiming to examine the effects of incorporating excess ice at the sub-grid scale to soil physics, i.e. whether different sub-grid scale distributions of excess ice differ reasonably from each other during excess ice melt. The results of single-grid simulations help to verify if the sub-grid representation of excess ice shows more potential in modeling excess ice compared to its previous version, where excess ice is homogeneously distributed in the CLM grid cell (Lee et al., 2014). We employ the forcing data at the North Slope of Alaska (NSA; 70° N, 156° W) and to the Northeast of Yakutsk (Yakutsk; 63° N, 130° E) to represent the continental and maritime types of climate respectively in the circum-Arctic. They have the annual mean temperature and precipitation close to each other, while the seasonal variability in temperature is smaller in the North Slope of Alaska due to its adjacency to the Arctic Ocean (Bieniek et al., 2012).

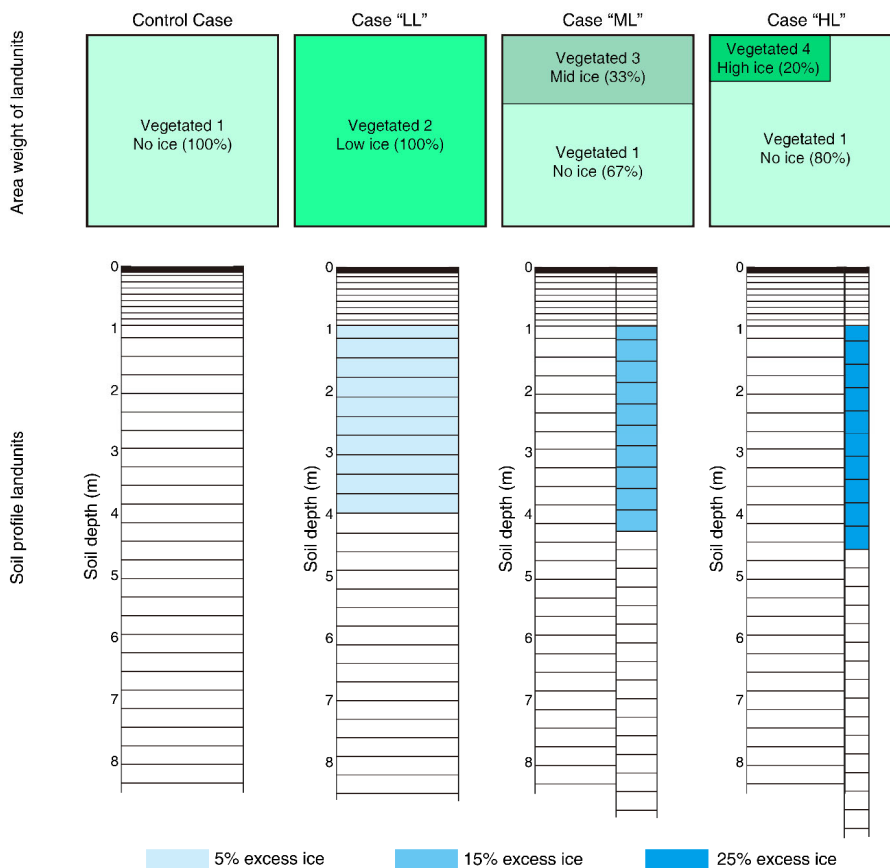


**Figure S1: The schematic figure for the area weights (the percentage between parentheses) and soil profiles within the landunits in the four single-grid simulations. Besides the control case, three other cases are with the same amount of excess ice within the single grid. “LL”, “ML”, and “HL” are abbreviations for “Low ice Landunit”, “Mid ice Landunit”, and “High ice Landunit”, representing the applied excess ice landunit in each case.**

The grid-mean volumetric excess ice content is set to be 5%. We set up three excess ice cases with the same (or very close) grid-scale excess ice content but with different spatial variability. For each site, we design three cases, having a 100% area weight of 5% volumetric excess ice content (NSA\_LL and Yakutsk\_LL), a 33% area weight of 15% volumetric excess ice content (NSA\_ML and Yakutsk\_ML), and a 20% area weight of 25% volumetric excess ice content (NSA\_HL and Yakutsk\_HL), respectively (Figure S1). For all of the original soil layers between 1-4 meters, excess ice is incorporated homogeneously, which proportionally increases the soil thickness for these layers. The initialization depth of excess ice keeps the same as in Lee et al. (2014). Both locations we choose are with 100% natural soil and continuous permafrost to avoid the interference of model results by other landunit types from the source.

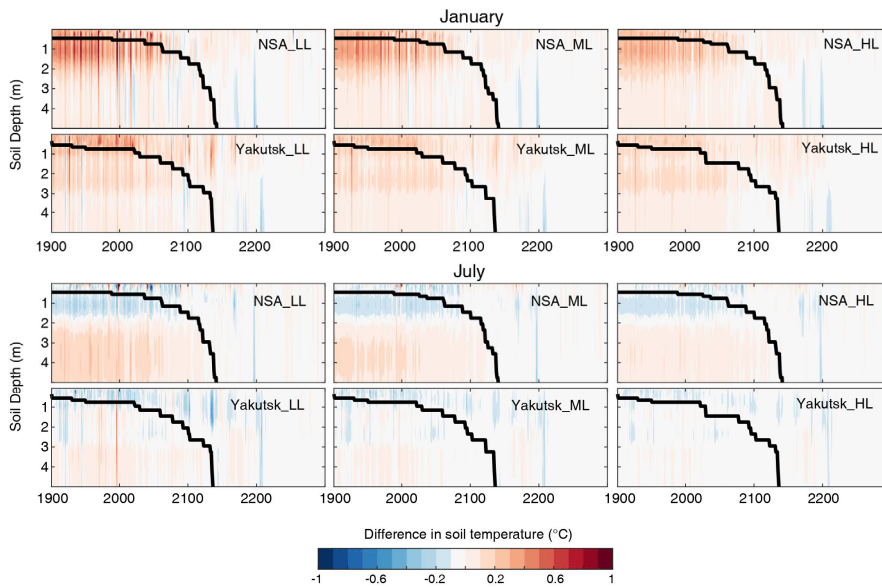


**Figure S2: Soil temperature differences from excess ice cases to control cases (NSA\_control and Yakutsk\_control) for the depth of 0.005-5 meters in January and July. Black lines are the active layer depth deepening through time. The active layer depth is calculated from grid-scale soil temperature for each case.**

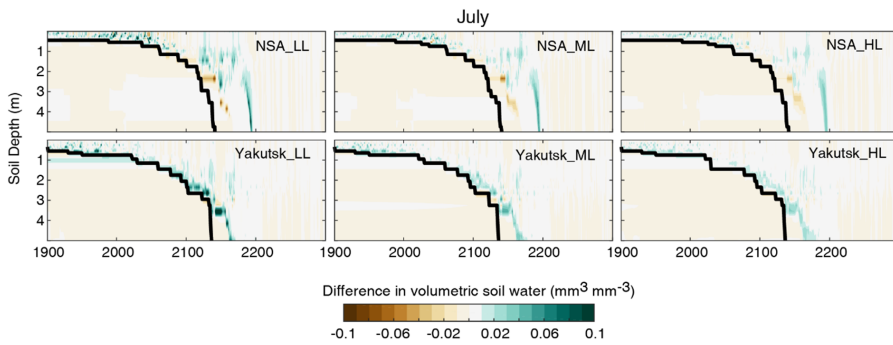


**Figure S3: Soil moisture differences from excess ice cases to the corresponding control cases (NSA\_control and Yakutsk\_control) for the depth of 0.05-5 meters in July. Black lines are the active layer depth deepening through time. The active layer depth is calculated from grid-scale soil temperature for each case.**

As a result, differences in soil temperature and moisture from excess ice cases to control cases in single-grid simulations quantitatively show the effects of excess ice and its melting. In the shallower layers (0-2 m), excess ice results in slightly higher soil temperature in January (winter) but lower soil temperature in July (summer) relative to control cases, reducing the magnitude of the seasonal cycle in soil temperature (Figure S2). In deeper layers (>2 m), the soil temperature in excess ice cases remains higher compared to control cases for both in summer and winter. The above responses in permafrost temperature results from the increases of specific heat and thermal conductivity of the soil layer after incorporating excess ice. As the climate warms and permafrost thaws, the meltwater discharges in the form of runoff, eventually bringing soil temperatures in excess ice cases closer to that in the control case. For soil moisture, the volumetric water content in July is higher in excess ice cases than control and is just above the permafrost table (Figure S3). As the active layer substantially deepens in the projected period for both sites, soil water in excess ice cases increases abruptly around 2180 for NSA while around 2150 for Yakutsk, indicating the degradation of permafrost in control cases. When permafrost degrades in the control case, the excess soil water in control cases starts to ~~of~~ runoff in the form of subsurface drainage, flushing out soil water and making the soil drier. Note that the subsurface drainage is unlikely to happen in reality since the permafrost at these two sites are much thicker than 10 m. Meanwhile, this has not occurred in excess ice cases yet, making the soil wetter in excess ice cases than in control cases. These responses in permafrost temperature and moisture after permafrost degradation are consistent with the results in Lee et al. (2014), suggesting that the excess ice physics developed in CLM4.5\_EXICE performs reasonably in a sub-grid manner in CLM5. Among the three excess ice cases, the “LL” case shows the strongest responses in both soil temperature and soil water content. On the other hand, the effects of excess ice in soil temperature and moisture are weaker in the “ML” and “HL” cases, where the same amount of excess ice is distributed more localized within a fraction of the grid.

Both sites exhibit active layer depth of around 0.5 m by the end of the spinup and active layer thickness does not increase substantially during the historical period (Black lines in Figure S2 and S3). For this reason, excess ice is incorporated one meter below the surface. No excess ice, therefore, melts during either the spin-up or the historical period simulations. Excess ice starts to melt around the 2070s in NSA\_LL, while the timing is delayed

for about 25 years in the other two cases for the same site (NSA\_ML and NSA\_HL; Figure S4). It is because the higher content of excess ice covering a smaller area takes longer to absorb enough latent heat of fusion from the atmosphere before it can start melting. Excess ice in NSA completely melts away in the 2170s and the exact timing of which varies slightly (< 5 years) between cases. In Yakutsk, excess ice starts to melt earlier, but with a slower rate compared to NSA. Similar to the NSA cases, Yakutsk\_ML and Yakutsk\_HL exhibit delays in the timing of excess ice melt compared to Yakutsk\_LL. Excess ice in Yakutsk\_LL completely melts in the 2170s, while the timings of excess ice melting in Yakutsk\_ML and Yakutsk\_HL is delayed for about 10 to 15 years, respectively (Figure S4).

Excess ice melting supplies extra water to subsurface water storage, increasing soil water and eventually converting to runoff. The increases in surface runoff correspond well in timing with excess ice melt (Figure S4). Earlier permafrost thaw timing in control cases causes an earlier increase in subsurface runoff and a decrease in the surface runoff than in excess ice cases. On the other hand, when the active layer depth reaches below the deepest soil layer in excess ice cases, more soil water from melt ice leads to the higher subsurface runoff compared to that in control cases. Among the three excess ice cases, the “LL” cases consistently exhibit the strongest and earliest responses in both surface and subsurface runoff as excess ice melts, being consistent with their earlier start of excess ice melt.

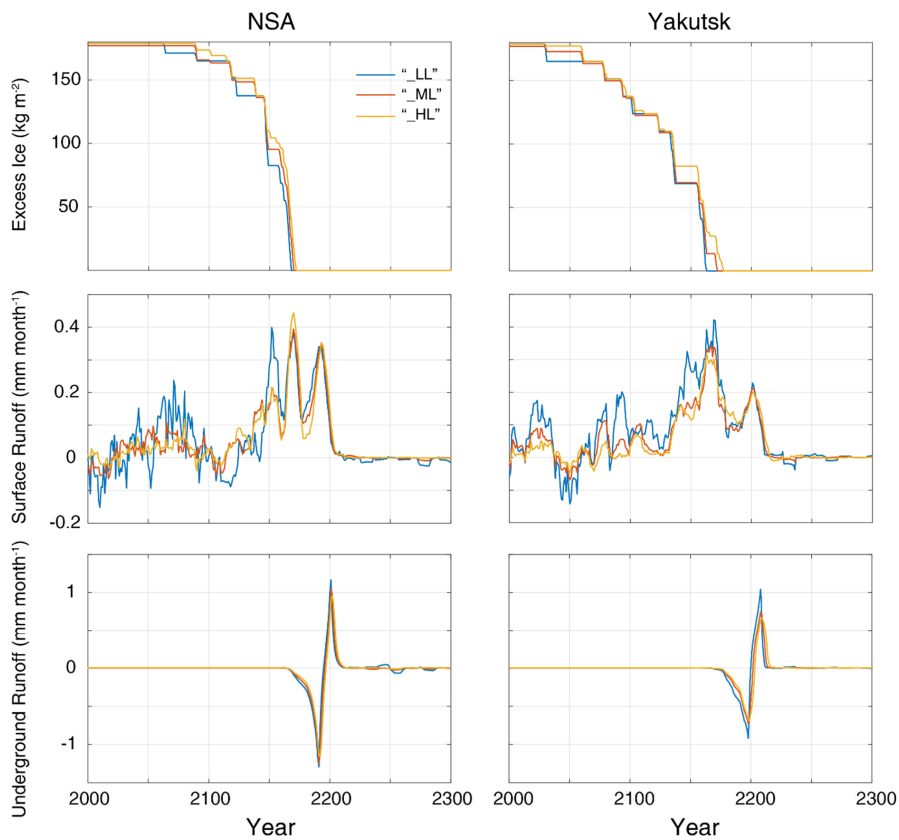


**Figure S4:** Time series of excess ice ( $\text{kg /m}^2\text{m}^{-2}$ ), as well as the difference of surface runoff ( $\text{mm /month}^{\pm}$ ) and subsurface drainage ( $\text{mm/month}$ ) from the three excess ice cases to control cases. A 15-year moving average is applied before plotting both the surface and underground runoff.

Formatted: Superscript

#### References

- Bieniek, P. A., Bhatt, U. S., Thoman, R. L., Angeloff, H., Partain, J., Papineau, J., Fritsch, F., Holloway, E., Walsh, J. E., Daly, C., Shulski, M., Hufford, G., Hill, D. F., Calos, S., and Gens, R.: Climate Divisions for Alaska Based on Objective Methods, *Journal of Applied Meteorology and Climatology*, 51, 1276-1289, 10.1175/jamc-d-11-0168.1, 2012.
- Lee, H., Swenson, S. C., Slater, A. G., and Lawrence, D. M.: Effects of excess ground ice on projections of permafrost in a warming climate, *Environmental Research Letters*, 9, 124006, 2014.